CERN-PPE/92-52
20 March 1992

EUROPEAN ORGANIZATION FOR NUCLEAR RESEARCH

Detection of Muons with a Lead/Scintillating-Fiber Calorimeter

D. Acosta[1)], S. Buontempo[2)], L. Calôba[3)], R. DeSalvo[4a)], A. Ereditato[2)], R. Ferrari[5)], G. Fumagalli[5)], G. Goggi[4,5)], W. Hao[6)]†, A. Henriques[4,7)], L. Linssen[4,4a)], M. Livan[8)], A. Maio[7)], M.R. Mondardini[9)], B. Ong[1)], H.P. Paar[1)], F. Pastore[5)], E. Pennacchio[5)], L. Poggioli[4,10)], G. Polesello[4,5)], F. Riccardi[2)], A. Rimoldi[5)], C.V. Scheel[4a,11)], J.M. Seixas[3,4)], A. Simon[12)], M. Sivertz[1)], P. Sonderegger[4)], M.N. Souza[3)], Z.D. Thomé[3)], V. Vercesi[5)], Y. Wang[6)]†, R. Wigmans[4)] and C. Xu[6)]†

1) *University of California, San Diego, USA*
2) *Università di Napoli and INFN Sez. Napoli, Italy*
3) *COPPE/EE/UFRJ, Rio de Janeiro, Brazil*
4) *CERN, Geneva, Switzerland*
4a) *CERN/LAA project, Geneva, Switzerland*
5) *Università di Pavia and INFN Sez. Pavia, Italy*
6) *Worldlab, Lausanne, Switzerland*
7) *LIP, Lisbon, Portugal*
8) *Università di Cagliari and INFN Sez. Cagliari, Italy*
9) *Cornell University, Ithaca, USA*
10) *LPNHE, Université Paris VI&VII, Paris, France*
11) *NIKHEF-H, Amsterdam, the Netherlands*
12) *Universität Heidelberg, Heidelberg, Germany*

† On leave of absence from IHEP Beijing, China

Abstract

We report on an experimental study of the signals from high-energy (5 - 225 GeV) muons traversing a 9.5 interaction lengths deep electromagnetic/hadronic calorimeter consisting of lead and scintillating plastic fibers, constructed at CERN in the framework of the LAA project. The muons lose on average between 2.6 GeV (at 5 GeV) and 8.8 GeV (at 225 GeV) in this process. This energy loss can be measured with a precision of a fraction of a GeV in most of the events. Accuracy in the energy loss measurements is important since the RMS spread in the energy loss of muons traversing this calorimeter is not smaller than $\sim$ 6% at any energy. The nominal calibration constants, derived from the calorimeter response to electromagnetic showers, are found to be incorrect for the muon signals. On average, these calibration constants are between 40% (for low energy muons) and 15% (high energy) too high. The fiber bunches sticking out of the back plane of the calorimeter for readout purposes cause the muon signals to be position dependent. This can cause an anomalous enhancement of the muon signal of up to 35%. A moderate position resolution of $\sim$ 1 cm is sufficient to correct for this effect. The e/mip ratio was found to be 0.72 ± 0.03.

(Submitted to Nuclear Instruments and Methods in Physics Research)

1. INTRODUCTION

Muon detection is an important aspect of modern experiments in particle physics. Much of the new physics envisaged at the future multi-TeV pp colliders LHC and SSC is believed to be accessible through the muon channels[1,2] . Accurate measurements of the muon momenta require a high-precision magnetic spectrometer. However, such a spectrometer is usually located behind a thick absorber (the calorimeter) intended, among other reasons, to absorb all the other particles. The muons will lose some fraction of their energy in this absorber. This fraction may fluctuate quite strongly from event to event, especially at high energies. In order to achieve the required measurement accuracy it is, therefore, important to measure this energy loss. Also, the ability to trace the muon through the absorber may be important, since it allows the linking of track information obtained from measurements made downstream and upstream from the calorimeter.

Although the prime task of the calorimeter concerns the detection of showering particles (electrons, γ's, hadrons) and missing energy (e.g. caused by neutrinos), it can also provide the muon information mentioned above. Because of their different emphases, calorimeters are usually not optimized for muon detection. The signals produced by muons are usually much smaller than the signals from particles for which this detector is intended and if the dynamic range is limited, for example because of the signal-to-noise ratio, muons may be barely detectable.

The Spaghetti Calorimeter (or SPACAL) was developed, in the framework of the LAA project at CERN, as a dedicated calorimeter for LHC/SSC experiments. It is an almost compensating lead/scintillating-fiber calorimeter with monolythic towers, i.e. without longitudinal segmentation into an electromagnetic (e.m.) and an hadronic section. Many of its properties are described elsewhere[3-10] .

The signal-to-noise ratio is excellent in this calorimeter. Muons traversing the 2 m deep detector produce signals of typically more than 1000 photoelectrons, while the noise occurs at the single-photoelectron level. In a previous study we showed that muons travelling only 0.3 nuclear interaction lengths through this detector could be usefully employed as a source of calibration signals[9] .

In this paper, we study the properties of this calorimeter with respect to the detection of muons. In section 2, the detectors used for these studies, their calibration and the experimental setup are described. Section 3 deals with the experimental data and with the event selection. Section 4 gives results on the energy, angular and position dependence of the muon signals, and on the accuracy with which the muon energy loss can be measured. Also the e/mip ratio, which determines the absolute sampling fraction for electromagnetic showers and which is important for understanding the compensation characteristics of this calorimeter, is determined in this section. A summary and conclusions are presented in section 5.

2. EXPERIMENTAL SETUP

2.1 The detector

The measurements were performed with 2 calorimeters consisting of longitudinally unsegmented towers. Each tower contains 1141 plastic scintillating fibers* with a diameter of 1 mm and a length of 2.20 m. These fibers form the active part of the sampling calorimeters. They are embedded in a lead matrix in such a way that each fiber is equidistant to its six neighbors (fig. 1a). The fiber spacing is 2.22 mm (center to center), such as to achieve a volume ratio lead:fiber of about 4:1, needed in order to make the calorimeter approximately compensating[8,11,12]

The fibers were grouped to form towers. Each tower has an hexagonal cross section (86 mm apex to apex). The depth of the lead structure is 200 cm. The fibers sticking out at one end of the tower were bunched together in an hexagonal structure, machined and polished and coupled through an hexagonal light guide (79 mm long, 42 mm apex to apex) to a photomultiplier (PM)** . The other ends of the fibers were polished and made reflective by aluminium sputtering, such as to make the response more uniform as a function of the position along the fiber. More detailed information about the structure of the calorimeters is given in ref. 4. The fact that part of the active material, on average 18 cm or 9%, is sticking out of the lead structure in a nonuniform (bunched) way has significant effects on the muon signals, as is shown in sect. 4.

The calorimeters consist of 155 and 20 towers, respectively, and will be called C155 and C20 in the following. In C155, a central tower is surrounded by 7 concentric hexagonal rings (see fig. 1b); with the outer ring incomplete, the detector has roughly a cylindrical shape with a diameter of 1 meter. In the tests described in this paper, this detector was installed as intended in experiments for which it was developed, namely with the fibers running in almost the same direction as the beam particles and the readout located at the back end of the detector. In this way, its dimensions amounted to 9.5 nuclear interaction lengths (λ_I) in depth and 4.8 λ_I across. Similar, dedicated, muon measurements were done at an earlier stage using the C20 calorimeter. This detector, a prototype for C155, consists of a central tower surrounded by 2 hexagonal rings and one extra tower (see fig. 1c).

The PM signals were handled as follows. The anode signal from the SPACAL towers was split into 2 equal parts by means of a passive splitter inside the base. One part went to the counting room where it was further fed into an active splitter, one output of which was sent unchanged into a 12-bit charge ADC, the other output was amplified by a factor ~ 10 before being fed into an ADC. The other half of the anode signal went into a linear adder, where it was combined with tower signals from the same hexagonal

* SCSF-38, produced by Kyowa Gas, now Kuraray Co. Ltd, Tokyo, Japan

** Philips XP 2282, 8-stage

ring. The resulting ring sum signals were treated in the same way as the signals that were directly sent to the counting room. The signals of C20 were only split at the ADC level, but not inside the PM base.

The gain in the PM tubes was set to deliver $\sim$ 4 pC/GeV in the central detector region, gradually going up to $\sim$ 20 pC/GeV in the outer rings of the C155 detector, for the unamplified channels. For the measurements in which C20 served as a leakage calorimeter, the gain of its towers was set to $\sim$ 10 pC/GeV. The ADC gain was 4 counts/pC. This procedure was chosen to circumvent the insufficient dynamic range of our PM/ADC system and to be sensitive to small energy deposits far away from the shower axis.

The data discussed in this paper were taken at an ADC gate width of 400 ns. Sparse data readout was enabled: signals smaller than 4 counts above the pedestal value were not recorded. This corresponds to a cutoff of 5 MeV energy deposits in the amplified channels of the outer rings of the C155 calorimeter, of 25 MeV for the central region of the C155 and C20 detectors, and of 10 MeV for the amplified C20 channels when it served as a leakage calorimeter.

2.2 The beam line

The measurements were performed in the H2 beam line of the SPS at CERN. The Spaghetti Calorimeter was mounted on a platform that could move horizontally and vertically with respect to the beam line, with a precision of about 1 mm. Moreover, the detector could be rotated around its vertical axis, so that the particles could be sent into the detector at a chosen angle θ_x (usually a few degrees) with respect to the fiber axis, in the horizontal plane. The precision of the angular movement was better than 0.1 mr , although the absolute value of the angle was only known to $\sim$ 10 mr[9] . In the C155 measurements, the calorimeter was oriented as indicated in figs. 1a,b, with the fiber layers in the horizontal plane. In the C20 measurements, the fiber layers were tilted by $\sim 10^0$ with respect to this plane, as indicated in fig. 1c.

About 12 cm upstream of the calorimeter, a preshower detector was mounted. This preshower detector (PSD) consisted of an absorber sheet (1.14 X_0 tungsten + 0.53 X_0 lead), followed by a scintillation counter (S6). The signal in this scintillator provided a clean (at energies above 40 GeV about a factor 10) separation between electron and pion/muon events[5] . Further upstream of the calorimeters, a trigger counter telescope was installed. It consisted of 5 scintillation counters (S1 - S5) and 2 drift chambers with x,y readout (BC1, BC2). In the C155 measurements, C20 was installed on a fixed platform behind C155, with the fibers running perpendicular to the beam. In this way, C20 served as a leakage detector, providing an extra 1.7 λ_I of *longitudinally subdivided*

calorimetry. This proved to be very useful for the identification of muons. The latter layout is shown in fig. 2.

In the H2 beam line, muons are a byproduct of the pion beams. Unlike pions and electrons, the muons from this beam line are *not* monoenergetic. They are produced in the decay of momentum selected pions (and kaons) and, therefore, they exhibit a rather broad spectrum. In first appproximation, the muon energy spectrum is flat, extending from $E \cdot (m_\mu/m_\pi)^2$ to E, with E being the energy of the momentum selected particles and m_μ/m_π the muon/pion mass ratio. The average muon energy is then approximately $0.8\ E$. When, in the following, we speak about muons of E GeV, we always mean muons from the decay of E GeV mesons.

Pure muon beams could be obtained by putting a sufficiently thick absorber far upstream into the beam line. Measurements with such pure beams were only performed with C20, for negative muons of 40, 80 and 225 GeV, which were sent into the calorimeter at a small angle θ_z with respect to the fiber axis. The beam particle rates were low, $\sim$ 50 events per spill. The spills lasted for 2.6 s and were repeated every 14 s. The calorimeter was triggered by a coincidence S1-S2-S3 (see fig. 2), leading to a beam spot with a diameter of $\sim$ 2 cm.

No such dedicated measurements were done with C155. In the present analysis we used muons that contaminated the pion beams. Especially at low energies ($<$ 40 GeV), such muons formed a considerable fraction of the beam. Data were collected for negative particles at 5, 10, 20, 40, 80 and 150 GeV. Except at the lowest energy, the calorimeters were triggered by a coincidence S1-S2-S3, yielding a beam spot with a diameter of $\sim$ 2 cm. At 5 GeV the rates were too small for such a trigger. In this case, only the coincidence S1-S2 was required, resulting in a very large beam spot (diameter $\sim$ 10 cm).

Except for $\theta_z = 0$, the particles were not sent into the center of the detector. The impact point was chosen in such a way, that the longitudinal center of gravity of the hadronic showers would lie on average on the central tower axis. In practice, this meant that the impact point was horizontally displaced from the detector axis by a distance of 12 mm $\times\theta_z$ (degrees).

Off-line event selection required a single track, by cutting on the pulse height of the scintillation counters S1,2,3 between 0.5 and 1.7 times the minimum ionizing particle (mip) value. The S6 signal was required to be smaller than 2 mip. The x and y coordinates measured in the two beam chambers had to agree within 1 cm. Beam halo particles were removed by cuts on x and y in the beam chambers. In the C155 measurements, where the detector was exposed to mixed π/μ beams, clean muon event samples could be obtained using the information from the C20 backing calorimeter, as described in sect. 3.

2.3 Calibration of the detectors

The calorimeters were calibrated with 40 GeV electrons. About 1500 electrons were sent into the central region of each of the 155+20 individual towers, at an angle θ_z of 3^0 to the fiber axis. In this way, the e.m. showers deposited on average $\sim$ 95% of their energy in the tower concerned. Off-line, the calibration constants (the relation between picocoulombs and GeV's for each individual tower) could be determined with a statistical precision of $\sim$ 0.3% from this data. Because of systematic effects, due to fiber-to-fiber response fluctuations, high-voltage instabilities, etc. the tower-to-tower calibration is much less precisely known, to about 3%[8] .

3. EXPERIMENTAL DATA AND METHODS

The results described in this paper were obtained by analyzing the following sets of data:

- Dedicated muon runs at 40, 80 and 225 GeV. The particles were sent into the C20 calorimeter at angles $\theta_z = 0^0, 0.5^0, 1^0, [1.5^0], [2^0], [2.5^0], 3^0, 4^0, [5^0]$ or $[6^0]$ with the fiber axis, where angles denoted in square brackets were only used at 225 GeV. Between 1500 and 3000 events were accumulated per run.
- Event samples of muons contaminating the pion beams at 5, 10, 20, 40, 80 and 150 GeV. These data were taken at angles $\theta_z = 0^0$ and 3^0 with the C155 calorimeter.
- A grid scan at 80 GeV, where muons (again as by-products of the pion beam) entered the C155 calorimeter at 49 different impact points at an angle $\theta_z = 2^0$, in contrast to the other mentioned data, where always one impact point was chosen, depending on the angle (see sect. 2.2). In total, 1500 muon events were accumulated in this run.

The dedicated muon beams, used to study the C20 signals, did not contain any contaminating particles. In order to create clean muon samples from the C155 tests, the contaminating electron and pion events had to be removed, in such a way that the resulting muon samples were minimally biased. The main tool for achieving this goal was the C20 calorimeter that served as a backing calorimeter in these tests. Muons produced very characteristic signals in this fine-grained detector. Figure 3 shows a typical example of the energy deposit pattern by a muon traversing this leakage calorimeter. In fig. 4, the distributions of the energy deposited in this calorimeter as a whole (fig. 4a) and in one of the individual towers (fig. 4b) by muons traversing it perpendicularly are shown. In order to be considered a muon, the particles were required to deposit between 125 MeV and 1.5 GeV in the leakage calorimeter, with the signal in individual towers not exceeding 300 MeV. Between three and six towers were required to have a signal of at least 25 MeV.

These requirements eliminated all the electron events, all the pion events contained in C155 and most of the pions that were not contained, in particular those in which a charged pion escaped C155[9] . The main remaining contamination consisted of pion events, where a muon was generated in the shower. The probability for this process is roughly proportional to the energy (about 2% at 150 GeV[9]) and, therefore, mainly the high-energy samples were contaminated. These remaining pion events were eliminated with two additional criteria based on the energy deposit pattern in C155 itself. The first criteria exploits the strong differences in the lateral energy deposit patterns between pions and muons. Muons lose their energy predominantly through ionization and produce, therefore, only signals in a very limited number of towers, contrary to showering pions. Muons travelling in a straight line at $\theta_z = 3^0$ always traverse either 2 or 3 calorimeter towers, depending on their impact point. The π/μ separation is illustrated in fig. 5, where the fraction (f_3) of the total C155 signal recorded in the three calorimeter towers that gave the largest contribution to it is plotted against the total C155 signal, for the particles from the 10 GeV beam. Most of the pions were eliminated by requiring f_3 to be larger than 75%, a cut that retains all the muon events, including those events in which the muons undergo a catastrophic energy loss, as could be checked with the dedicated muon data, which contained no contaminating pions. The second criterion exploits the fact that muons only lose a fraction of their energy in C155, while pions are usually fully absorbed. Therefore, the muon signals are smaller than the pion ones, especially at high energy. This is illustrated in fig. 6, which shows a scatter plot of the signals for 80 GeV particles. The signal in the leakage detector is shown versus the signal in the main calorimeter. Clearly, a cut on the signal in the latter is a very efficient means of separating pions from muons. Since we did not want to truncate the Landau tail of the muon signal distribution, the cut on the total C155 signal was applied last, it was only applied for $E \geq 40$ GeV and chosen at the highest possible energy. Figure 6 also shows that all muons produce a non-zero signal in the leakage calorimeter, clustering around 400 MeV (see also fig. 4a), while a large majority of the pions are fully contained in the C155 detector (zero in the leakage calorimeter). The numbers of muon events from the various C155 data samples that were used for the present analysis and, when relevant, the energy dependent cut on the total C155 signal are listed in table 1.

4. EXPERIMENTAL RESULTS

4.1 The energy dependence of the muon response

For angles $\theta_z = 0^0$ and 3^0, muon data were available at 7 different energies: 5, 10, 20, 40, 80, 150 and 225 GeV. In fig. 7, the signal distributions for muons of different energies traversing the 9.5 λ_I deep Spaghetti Calorimeter at $\theta_z = 3^0$ are shown. Two trends are clear from this figure. When the muon energy increases, the most probable

(*mop*) value of its energy loss shifts gradually to larger values and the signal distribution gets more pronounced high-energy tails. The latter feature, particularly striking at 225 GeV, is due to higher-order quantum-electrodynamic (QED) effects, like bremsstrahlung or direct e^+e^- pair production, which become important when the muon energy is of the same order as the critical energy ($\sim$ 250 GeV in lead). Similar phenomena were observed by the HELIOS Collaboration[13] , who measured the signals from 8 - 200 GeV muons in their ^{238}U/plastic-scintillator calorimeter.

From these distributions, we determined both the average and the most probable values of the signals. The latter were obtained by fitting the signal distributions to a Moyal function[14] , which approximates the Landau distribution. The conversion of the signals (in pC) to energy (in GeV) was made on the basis of the calibration constants found with electrons, not correcting for any instrumental effect. The results are listed in tables 2a and 2b for $\theta_z = 0^0$ and 3^0, respectively. The tables also list the $\sigma_{\rm RMS}$ values of the distributions, which are a measure for the uncertainty in the energy loss in case it can not be explicitly measured, which may occur in experimental situations when a muon traverses the absorber (calorimeter) in the vicinity of a showering particle. In fig. 8, the average and most probable values for the energy loss are shown as a function of the beam energy, for $\theta_z = 3^0$. Figure 9a shows the average fraction of the energy lost by the muons when traversing the calorimeter and fig. 9b the RMS width of the energy loss distribution as a fraction of the muon energy. These results demonstrate that, although the average *fraction* of the muon energy lost in this calorimeter continuously decreases as a function of the energy, the RMS *spread* of the fractional energy loss levels off at $\sim$ 6%. Therefore, unless the calorimeter offers the possibility to measure this energy loss event-by-event with adequate precision (e.g. 10-20% in the high energy tail of the distribution), it will be this factor that limits the precision of muon momentum measurements rather than the quality of a muon spectrometer placed downstream.

It should be emphasized once again that all the results shown in figs. 7-9 and in tables 2a,b were obtained under the assumption that the measured muon signals may be converted into energy deposit using the calibration constants obtained from the calorimeter response to e.m. showers. The question arises to what extent it is correct to apply these calibration constants for calculating the energy loss by muons. It is well-known that the sampling fractions for e.m. showers and minimum ionizing particles may be quite different, especially in high-Z calorimeters[11] . Also, there are instrumental effects, coming from light attenuation in the fibers and from the fact that fibers sticking out of the absorber may contribute to the signal, which make this a questionable procedure. We will come back in detail to these points in sections 4.3-4.5, but already here we mention that the average and the most probable energy losses by muons presented in this subsection are *overestimated* by an energy dependent factor which ranges from $\sim$ 1.4 at low energy to $\sim$ 1.15 at the highest energies considered in

this study.

4.2 Angular effects

The angular dependence of the muon signals was studied with dedicated muon beams at 40, 80 and 225 GeV sent into the C20 calorimeter. The average signals are shown as a function of the angle θ_z in fig. 10. There is clearly an angular effect for $\theta_z < 1^0$. At $\theta_z = 0^0$, the average signals are systematically larger, by about 20%, than the signals for angles larger than 1^0. A striking exception occurs for $\theta_z = 5^0$, at which angle only 225 GeV data were available. Data at $\theta_z = 0^0$ and 3^0 were also available for the C155 measurements. In fig. 11, the ratio of the average signals measured at these angles is shown as a function of the beam energy for all data, confirming the effect that the signals at $\theta_z = 0^0$ are systematically larger. It should however be noted that at low energies (5 and 10 GeV) the discrepancy between the average signals at $\theta_z = 0^0$ and $\theta_z = 3^0$ is considerably smaller than at the other energies.

Angular effects for very small values of θ_z were observed before in the detection of e.m. showers[4,8] . These effects were, however, clearly of a different nature. It was observed that the energy resolution, and in particular its energy independent component (the constant term), rapidly deteriorates as a function of θ_z for $\theta_z < 3^0$. Also, the signal distributions become asymmetric for $\theta_z < 1^0$. These effects were attributed to the fact that the contribution of the early, strongly collimated shower component to the calorimeter signal depends sensitively on the impact point of the particles (lead or fiber), given the relatively small number of different fibers that effectively contribute to the signal. However, contrary to muons, the average calorimeter signal for e.m. showers was observed to be constant to within one percent as a function of the angle.

The origin of the anomalously large muon signals at $\theta_z = 0^0$ is the readout part of the calorimeter. As will be shown in the next subsection, the clue to the explanation of the observed effects is provided by the anomalies at $\theta_z = 5^0$ (fig. 10) and at low energies (fig. 11).

4.3 Effects of penetrating muons

Contrary to showering particles, muons do not get absorbed in this calorimeter. They lose some fraction of their energy and then leave the detector through its back plane. That is where the signal readout is located. The scintillating fibers, composing the active calorimeter material, extend out of the back plane over a distance of ~ 18 cm and are bunched together in order to be read out. This is shown in detail in fig. 12. After traversing the absorber part of the calorimeter, the muons may also produce a signal in this bunch of fibers. Clearly, such a signal depends on the exit position and angle of the particles. It will be largest for muons traversing the back plane in the center

of a tower and practically zero for muons exiting near the boundary between different towers. Except at low energy, where multiple scattering causes smearing effects, there will be a strong correlation between the point at which the muon leaves the calorimeter and the impact point. Therefore, one may expect the muon signals to be position dependent.

This was investigated using the muons from the matrix scan (table 1). Muons of 80 GeV were sent into the C155 calorimeter at an angle of 2^0. The beam was steered into 49 different impact points, located on a 7×7 matrix with a period of 4 cm. Assuming that the particles travel in a straight line, one may calculate their exit points. In the lateral detector plane, this will be horizontally displaced over a distance of $200 \times \tan(2^0) = 7.0$ cm with respect to the impact point. The location of the various exit points is indicated in fig. 13. The position of the fiber bunches is also shown in this figure.

The average muon signals are shown as a function of the position of the exit point with respect to the nearest tower center in fig. 14. Because of the limited statistics and the fact that the matrix period of 4 cm approximately corresponds to half of the (apex-to-apex) size of a calorimeter tower, which means that the same distance from exit point to tower center occurred for several impact points, the data sets were grouped together for this analysis (see fig. 13). From fig. 14, the effect described above is very clear. Muons exiting the calorimeter at the center of a tower produce a signal that on average is $\sim 35\%$ larger than for muons that leave the detector near a tower edge.

The angular effects described in the previous subsection can be explained from the same phenomenon. In fig. 15, the (average) impact and exit points of the muons during the angular scans are indicated, together with the position of the fiber bunches. It turns out that the muons in the $\theta_z = 3^0$ exposures left the calorimeter on average near the boundary between two towers, while the muons in the $\theta_z = 0^0$ runs were steered into a tower center, producing a signal that at high energies is on average $\sim 20\%$ larger (figs. 10,11). Figure 15 also shows that another case for which the exiting muons pass through a fiber bunch occurs for $\theta_z = 5^0$. Indeed, a similar increase in the muon signal was observed at this angle (fig. 10).

The fact that the signal ratio for $\theta_z = 0^0$ and $\theta_z = 3^0$ is smaller than the value of 1.35 expected from the matrix scan is most likely due to the fact that the 0^0 measurement did not exactly correspond to the maximum of the curve in fig. 14. As was pointed out in sect. 22.2, the angle θ_z was only known with a precision of ~ 10 mr, which translates into a systematic uncertainty in the lateral coordinates of the extrapolated exit point of about 20 mm. At low energies, the difference between the average signals at $\theta_z = 0^0$ and $\theta_z = 3^0$ was observed to vanish (fig. 11). This is due to multiple scattering, which disturbs the correlation between the impact and exit points. Multiple scattering in this 278 X_0 deep calorimeter leads to a deviation from the straight line extrapolation, which

in the back plane amounts on average to $\sim 60/E_\mu$ cm, with E_μ in GeV, so that the uncertainty in the exit point coordinates is actually larger than the diameter of one tower for 5 GeV muons. Therefore, the 5 and 10 GeV data will always be affected by this enhancement, no matter the value of θ_z.

The effects found from the matrix scan analysis can also be quantitatively understood. Plastic makes up 18.4% of the detector volume. This means that muons traverse on average 37 cm of fiber on their way through. The fibers extend 18 cm beyond the calorimeter volume and occupy a fraction of the space containing them that gradually increases from 18.4% close to the calorimeter to 78.5% ($\pi/4$) close to the light guide. Muons exiting through a tower center will therefore on average see an additional 8.7 cm of plastic. This, together with the fact that the signal for light produced close to the light guide is on average about 40% larger than for light produced inside the absorber volume, because of light attenuation in the fiber (1), leads to an expected signal increase of at maximum $(8.7 \times 1.4)/37 = 33\%$. Similarly, one may calculate the average increase in the muon signals due to this effect. The fibers sticking out of the calorimeter correspond to 9% of the fibers inside the absorber volume. Combined with the factor 1.4 from light attenuation, this leads to an average effect of 12-13%.

The data from fig. 14 were obtained at 80 GeV. There are reasons to assume that these penetration effects are relatively more important at high energies, i.e. at energies where bremsstrahlung is an important energy loss mechanism. If a shower created by an energetic bremssstrahlung γ were incompletely contained, the numerous escaping shower particles would cause a considerable signal increase, because of the strongly different shower sampling fractions inside and outside the absorber volume. This effect was clearly observed in detectors that were only a few cm too short to fully contain e.m. showers[4] . At low energy, bremsstrahlung is negligible and, therefore, the penetration effects on the signals are presumably smaller than the ones observed at 80 GeV.

Obviously, a position dependent signal is an undesirable feature for a particle detector. In this case, there are several recipes to deal with this problem. In one approach, one may change the construction of the calorimeter in such a way that no active material is sticking out of the absorber volume. The signals will then have to be transported to the light detector through a tapered light guide or through clear (undoped) fibers connected somehow to the active ones. In another approach, one may correct the observed signals for this effect using the information from fig. 14 and knowledge about the impact point of the muons. Given the uncertainties coming from multiple scattering in the detector, the position resolution need not be better than ~ 1 cm for this purpose.

4.4 The e/mip ratio

In this and the next subsection we discuss the absolute value of the calorimeter signals. First, we will try to determine the so-called *e/mip* ratio. This ratio relates

the signals from e.m. showers to those of minimum ionizing particles depositing the same amount of energy in the calorimeter. Since the sampling fraction and the amount of energy lost in the detector by a *mip* are precisely known from the composition of the calorimeter and from the specific ionization losses ($< dE/dx >$) in the various materials composing it, a measurement of the e/mip value is equivalent to an absolute measurement of the sampling fraction for an e.m. shower. This parameter is important in view of understanding the precise e/h value of the calorimeter[11,15] . It should be emphasized that a *mip* is a *hypothetical particle*, it does not exist. But since a muon is the closest thing to a *mip* that nature provides us with, we use the muon data for doing this analysis, following the examples set by the HELIOS[13] and ZEUS[12] Collaborations.

Our calorimeter consists of 77.7% lead, 18.4% plastic and 3.9% air, and is in total 200 cm long. According to the Particle Data Book[16] , a *mip* deposits on average 2067 MeV in this structure, out of which 74.0 MeV goes into the plastic. The plastic fibers consist of a polystyrene scintillating core, surrounded by an acrylic cladding. The cladding is 29 μm thick, for a total fiber diameter of 1 mm, and represents therefore 11.3% of the plastic. Ultraviolet light produced in this cladding might travel into the doped fiber core and there be absorbed and reemitted in the visible region, but it is unknown to what extent such a mechanism contributes to the measured signals. If the energy deposited in the fiber cladding did not contribute at all to the measured signal, the sampling fraction for a *mip* would amount to $74.0 \times (1 - 0.113)/2067 = 3.18\%$. This fraction would increase to $74.0/2067 = 3.58\%$ if the cladding energy contributed in the same way to the signals as the energy deposited in the fiber core. This peculiarity of scintillating fibers leads thus to an intrinsic uncertainty in the absolute sampling fraction. In the following determination of the e/mip ratio, we assume that all the energy deposited in the plastic (74 MeV) contributes in the same way to the measured signals. Separately, we investigate to what extent the mentioned uncertainty in the sampling fraction contributes to the error on the experimental e/mip result.

From table 2b, we see for example that 10 GeV muons deposit on average 4.07 GeV in the calorimeter. This result is based on a calibration of the detector with e.m. showers and one could, therefore, interpret it as a measurement of e/mip being $2.067/4.07 = 0.51$. This is, however, an oversimplification. First of all, there are instrumental effects that work out differently for the electron and muon signals. One such effect, caused by the fibers sticking out of the back plane, was already discussed in sect. 4.3. As was shown there, one can avoid this effect by analyzing the data taken at $\theta_z = 3^0$, which did not show an enhanced energy deposit. Another instrumental effect is due to light attenuation in the fibers. The electron signals are produced by scintillation light that is generated not far (typically 5 cm) from the front face of the calorimeter. Therefore, these signals are much more affected by light attenuation than the muon signals, which are caused by light that on average originates from the center of the calorimeter. The

attenuation characteristics of the fibers are well described by the following formula[8] :

$$I(z) = C[e^{-z/11.0} + 0.85\, e^{(z-4.4)/11.0} + 1.22\, e^{-z/0.77}] \quad (1)$$

which expresses how the signal I changes as a function of the distance z (in meters) to the PM. From this, one may calculate that, for equal energy deposits, e.m. shower signals are on average 15% smaller than muon ones, just because of the effects of light attenuation. When the calibration of the calorimeter by means of electrons is chosen as the basis for the energy scale, the energy deposited by muons (table 2) has to be multiplied by 0.85 in order to account for this effect. Therefore, $e/mip = 2.067/(4.07 \times 0.85) = 0.60$ is a better estimate of the value we want to determine.

However, also this result is not correct, since 10 GeV muons are by no means minimum ionizing particles. Even the lowest-energy muons used in these tests are extremely relativistic ($\gamma > 25$). The energy loss per unit length may be considerably larger than the minimum ionizing value for such relativistic muons[17] . This is due to phenomena such as δ-ray emission (relativistic rise), bremsstrahlung, e^+e^- pair production and, at very high energies, nuclear reactions. The contribution of these effects to the total energy loss is strongly dependent on the muon energy and on (the Z value of) the material. The energy dependence may be illustrated by fig. 8. The evaluation of the consequences of these effects for the muon signals, thereby unfolding the *mip* part of these signals, in a sampling calorimeter consisting of materials with very different Z values (lead, plastic) is a largely non-trivial problem. We mention two examples of the complications that occur.

a) For the calorimeter signal, one would expect the relativistic rise curve for plastic to be the relevant piece of information. However, some of the δ-electrons which are much more abundantly produced in the lead may escape and contribute to the signal as well. The relative importance of this effect cannot be calculated analytically.

b) When a high-energy muon radiates an energetic bremsstrahlung photon, this will develop an e.m. shower that is sampled in the same way as other e.m. showers are sampled by the calorimeter. The sampling fraction for this energy loss component may therefore be quite different from the sampling fraction for the *mip* part. Again, it is unclear how to deal with this complication in an analytical way.

We decided to approach this problem with a Monte Carlo program (GEANT 3.14)[18] that simulates the transport of muons through the calorimeter structure, taking into account all the details of the processes mentioned above. The program calculated for each muon energy the average amount of energy deposited in the fibers, which can then be compared to the 74.0 MeV mentioned before for a *mip*. If $\overline{\Delta E}_{fiber}$ is the average

energy loss predicted by this program and $\overline{\Delta E}_{mip} = 74.0$ MeV the average energy loss for a *mip*, the e/mip ratio can then be calculated as

$$e/mip = \frac{2.067}{\overline{\Delta E}_{\mu}(\lambda_{att} = \infty)} \times \frac{\overline{\Delta E}_{fiber}}{\overline{\Delta E}_{mip}} = 32.96 \frac{\overline{\Delta E}_{fiber}}{\overline{\Delta E}_{\mu,meas}} \qquad (2a)$$

with $\overline{\Delta E}_{\mu}(\lambda_{att} = \infty) = 0.85\overline{\Delta E}_{\mu,meas}$. This procedure allowed us to determine the e/mip ratio for each energy.

The e/mip ratio is an energy independent constant characterizing the calorimeter. If the program used to evaluate the non-*mip* part of the signals is correct, the resulting e/mip values should therefore be energy independent as well. The results, shown in table 3 and fig. 16, demonstrate that this internal consistency criterion is well met. A weighted average of the values obtained at the 7 different energies yields $e/mip = 0.717 \pm 0.006$.

The experimental uncertainty in the e/mip value is completely determined by systematic effects and is definitely larger than the 0.8% just mentioned. The main sources of systematic errors are the penetration effects discussed in sect. 4.3, the uncertainties concerning the experimental muon spectra, the uncertainty in the absolute sampling fraction (the role of the cladding light discussed before) and the Monte Carlo dependent correction that accounts for the non-*mip* part of the calorimeter signals.

By using the data taken at $\theta_z = 3^0$, we tried to eliminate the penetration effects as much as possible. At high energies, this is probably adequate, but at 5 and 10 GeV effects of the order of 10% have to be expected because of smearing due to multiple scattering. Such effects would lead to an overestimation of $\overline{\Delta E}_{\mu,meas}$ and hence to an underestimation of e/mip. This effect is counterbalanced by another one, coming from the muon spectra. The muon spectrum from 5 GeV pion decay is in first approximation flat between 3 and 5 GeV. Minimum ionizing particles deposit already more than 2 GeV in the calorimeter. Moreover, in order to be selected as a muon, the particles were required to traverse the backing calorimeter, which needs another 0.4 GeV. As a consequence, events from the Landau tail were systematically discarded in this analysis, which leads to an underestimation of the *average* muon signal $\overline{\Delta E}_{\mu,meas}$.

Another potential source of systematic errors in the e/mip value is the GEANT Monte Carlo used to evaluate the non-*mip* part of the calorimeter's muon signals. The measured signals are corrected by a factor $\overline{\Delta E}_{fiber}/\overline{\Delta E}_{mip} = 1 + \overline{\Delta E}_{non-mip}/\overline{\Delta E}_{mip}$, which is extremely energy dependent. Table 3 shows that $\overline{\Delta E}_{non-mip}/\overline{\Delta E}_{mip}$ amounts only to $\sim 10\%$ at 5 GeV, while at 225 GeV it is about a factor of 2! If the calculation of $\overline{\Delta E}_{non-mip}/\overline{\Delta E}_{mip}$ were wrong by for example 50%, the resulting e/mip value would therefore change only by 5% at 5 GeV, but by 50% at 225 GeV and fig. 16 would look very different.

Also the uncertainty in the absolute sampling fraction, stemming from the unknown contribution of energy deposited in the fiber cladding to the measured signals, may contribute to the systematic error in e/mip. In our determination of e/mip, we assumed that energy deposited in the cladding contributes in the same way as energy deposited in the fiber core. In the other extreme case, the cladding would be completely passive and the energy deposited by a *mip* in the active material would be $\sim$ 66 MeV, 11.3% less than assumed in our determination of e/mip. We developed a version of the GEANT program that includes the fiber cladding in its geometry description and found that the results for $\overline{\Delta E}_{fiber}$, representing here the average energy deposited by real muons in the fiber *core*, were systematically $\sim$ 10% lower than the values listed in table 3a, to be compared to the 11.3% mentioned above. This means that the uncertainty concerning the cladding light only leads to second-order effects of at maximum 1-2% on the e/mip value, because this uncertainty has in first order the same effects on the electron and muon signals and cancels in $(2a)$. The contribution of this effect to the systematic error on the e/mip value is therefore 1-2%.

In order to be less sensitive to the mentioned sources of systematic effects, we repeated the analysis using the *most probable* values for the energy loss instead of the average ones. Using the data from ref. 19, a *mip* loses most probably 1.882 GeV in this calorimeter, out of which 63.3 MeV are deposited in the plastic. The e/mip ratio can thus be calculated as

$$e/mip \;=\; \frac{1.882}{\Delta E_{\mu}^{\rm mop}(\lambda_{att}=\infty)} \times \frac{\Delta E_{fiber}^{\rm mop}}{\Delta E_{mip}^{\rm mop}} \;=\; 34.97 \frac{\Delta E_{fiber}^{\rm mop}}{\Delta E_{\mu,meas}^{\rm mop}} \qquad (2b)$$

The results of this analysis are given in table 3b. Indeed, the Monte Carlo dependent correction that accounts for the non-*mip* character of the muons is much smaller in this case (see also fig. 8). At 5 GeV, $\Delta E_{non-mip}^{\rm mop}/\Delta E_{mip}^{\rm mop}$ is only 4%, compared to 10% for the average energy loss, and also at the highest energies this correction factor is reduced by more than a factor of 2. Since the most probable value of the energy loss is much less energy dependent than the average one, the effects of the uncertainty in the muon energy are also greatly reduced.

The results on the e/mip value, which are also shown in fig. 16, are in very good agreement with the ones from the previous analysis. A weighted average of the values obtained at the seven different energies yields $e/mip = 0.713 \pm 0.006$, within 1% of the previous value. The largest deviations from this average value occur at the lowest and highest energies (-3.4% at 5 GeV, $+7.6\%$ at 225 GeV). The deviation at high energy is completely explained from the fact that the beam energy is not equivalent to the muon energy. If we do the calculation assuming 180 GeV instead of 225 GeV, the e/mip value decreases from 0.767 to 0.703, in excellent agreement with the average value. The deviation at low energy is most likely due to the penetration effects, as discussed before.

We conclude from this analysis that the systematic uncertainties affecting the value of e/mip are well under control and we evaluate our final result as

$$e/mip = 0.72 \pm 0.03 \tag{3}$$

The corresponding sampling fraction for e.m. showers varies between $2.29 \pm 0.10\%$ and $2.57 \pm 0.11\%$, depending on the contribution of energy deposited in the fiber cladding to the shower signals.

In the simulations that led to the chosen lead:fiber volume ratio as a means to achieve compensation, e/mip was assumed to be 0.60[11] . The present result may well explain why the compensation condition was not completely met (e/h turned out to be 1.15 ± 0.02[8]). Additional evidence for this explanation comes from Bernardi *et al.*,[12] who measured $e/mip = 0.67 \pm 0.03$ and $e/h = 1.05 \pm 0.04$ for a lead/scintillator calorimeter with the same volume ratio of passive and active material (10 mm Pb/2.5 mm plastic). The larger e/mip value observed in our fiber calorimeter is most likely due to a more efficient sampling of the very soft γ's abundantly produced in the shower development[11,15] .

4.5 Interpretation of the muon signals

The final question that needs to be answered is how to convert the observed muon signals into an energy loss, which after all is the purpose of a calorimeter. The energy loss distributions based on the calibration constants derived from the e.m. shower response are shown in fig. 7. We used the Monte Carlo program mentioned in the previous subsection to reproduce these signal distributions. For this purpose, the (smearing) effects of light attenuation in the fibers (sect. 4.4) on the muon signal distributions were included in the simulations. The simulated signals were multiplied with an overall scaling factor (μ_S) that served as a parameter in the program. Its value was determined from a comparison between the measured and simulated energy loss distributions.

As illustrated in fig. 17, the experimental energy loss distributions could be quite accurately described by the simulation program. The values of μ_S and the resulting values of e/μ, which are the factors by which the nominal calibration constants (e.g. 0.25 GeV/pC) have to be multiplied in order to find the energy loss corresponding to a given muon signal, are listed in table 4. In order to find proper values for the average and the most probable muon energy loss in the calorimeter and for the RMS width of the energy loss distribution, these numbers in table 2b have to be multiplied by the corresponding factor e/μ, which lies in the range $\sim 0.7 - 0.9$. For example, at $\theta = 3^0$, the muons lose on average between 2.6 GeV (at 5 GeV) and 8.8 GeV (at 225 GeV) when traversing this calorimeter, whereas the most probable energy loss varies between 2.3 GeV (at 5 GeV) and 4.8 GeV (at 225 GeV). As was pointed out in sect. 2.2, the

muons used for these studies were not monoenergetic. Their average energy amounted to ~ 0.8 times the nominal beam energy and, therefore, the average *fractional* energy loss $\overline{\Delta E_\mu}/E_\mu$ and the average *fractional* width of the energy loss distribution $\sigma_{\rm RMS}/E_\mu$ given in table 2 happen to be approximately correct.

The energy dependence of the factors e/μ illustrates one of the basic problems in interpreting the muon signals from this calorimeter. The response to ionizing particles is quite different from the shower response and since (bremsstrahlung) showers play an increasingly important role at higher energies, the calibration constants are energy dependent as well. These calibration constants are averages, with large event-to-event fluctuations, depending on the relative contributions from ionization and radiation to the signal. In practice, the best approach to calculating the energy deposited by individual muons is probably to assume that part of the signal (equivalent to the most probable response to a low-energy muon) is caused by ionization and the rest is due to radiation. The ionization part gets then a weighting factor of $(e/mip)/0.85$, whereas the remaining radiation component gets the same calibration constant as e.m. showers, again divided by 0.85 to account for light attenuation.

The experimental uncertainty in the energy loss obtained from a given muon signal is determined by sampling fluctuations and, therefore, probably similar to the energy resolution for an e.m. shower of the same energy. We found this resolution to be $\sigma/E = 12.9\%/\sqrt{E} + 1.2\%$ [8] , so that the energy loss by individual muons is measured with a precision of $\sim 7\%$, or a fraction of a GeV, at least for the events where ionization losses dominate. At higher energies, radiation becomes a more and more important energy loss mechanism. Unlike the ionization, this radiation occurs at random depths inside the calorimeter. Since no depth information is available for muons traversing this detector, and because of light attenuation in the fibers, an extra uncertainty in the measurement of the energy deposited in this way arises. In the worst possible case of emission of only one hard bremsstrahlung photon at a random depth, this uncertainty amounts to 14%, as derived from the light attenuation characteristics of the fibers (1). If the muon radiates several lower-energy γ's, the precision of the energy loss measurement improves accordingly.

In summary, the energy loss ΔE is measured with a precision of $\sim 7\%$ for $\Delta E \sim$ 3 GeV, gradually going up to $\sim 10\%$ at 10 GeV, $\sim 13\%$ at 20 GeV, to 14% at 50 GeV and beyond.

5. SUMMARY AND CONCLUSIONS

We have studied the signals from muons in the energy range 5 - 225 GeV traversing a 9.5 interaction lengths deep lead/scintillating-fiber calorimeter. The average energy deposited by these muons in the calorimeter varies between 2.6 GeV (at 5 GeV) and

8.8 GeV (at 225 GeV). The calorimeter usually measures this energy loss in individual events with a precision of a fraction of a GeV, except in the case of catastrophic energy losses where the precision of the measurements may drop to $\sim$ 14%, due to the lack of depth information and to light attenuation in the fibers. Because of higher-order QED processes, the RMS spread in the fractional energy loss of muons traversing this calorimeter does not drop below $\sim$ 6% at any energy, which illustrates the need for relatively precise calorimetric measurements of this energy loss.

The fiber bunches sticking out of the back plane of the calorimeter cause the muon signals to be position dependent. Muons exiting the detector in the center of a tower produce a signal that is on average up to $\sim$ 35% larger than for muons leaving the detector near a tower edge. A moderate position resolution of $\sim$ 1 cm is sufficient to correct for this effect.

When the nominal calibration constants, derived from the response to e.m. showers, are used, the muon energy loss found from the calorimeter signals is systematically too high, by an amount decreasing from $\sim$ 40% at 10 GeV to $\sim$ 15% at 225 GeV. This is due to instrumental effects (light attenuation in the scintillating fibers) and to the fact that the calorimeter response to showers and that to ionizing particles are not the same. The calorimeter response to e.m. showers was found to be $\sim$ 30% smaller than the response to minimum ionizing particles ($e/mip = 0.72 \pm 0.03$). This may well explain why the calorimeter is slightly undercompensating ($e/h = 1.15$). In spite of the fact that the interpretation of the muon signals is much less straightforward than for showers, and the results hence less accurate, the information that this calorimeter can provide on muons traversing it may be very valuable for the study of these particles in experiments in which they are produced.

Acknowledgements

We are deeply grateful to the LAA Project Leader, Prof. A. Zichichi, for his vision, his warm interest and his encouraging support. We thank our colleagues from the UA2 Group, and in particular P. Jenni and L. Mapelli, who helped us in many ways, in particular when running the beam tests. The work described in this paper would have been impossible without the outstanding technical support provided by our technicians O. Barnaba, C. Baudoin, M. Borriello, S. Bricola, J.-M. Chapuis, C. Farella, B. Foligne, A. Freddi, G. Improta, G. Iuvino, F. Pagano, S. Robinson, R. Rocco, L. Rose-Dulcina, G. Sannier, C. Schillinger, A. Sigrist and V. Vanzanella. Financial support from the Stichting voor Fundamenteel Onderzoek der Materie to the NIKHEF group, from the Istituto Nazionale di Fisica Nucleare to the Cagliari, Napoli and Pavia groups, from the Junta Nacional de Investigaçao Científica of Portugal to the Lisbon group, from the Conselho Nacional de Desenvolvimento Cientifico e Tecnologico of Brazil to the

Rio de Janeiro group, and from the U.S. Department of Energy and National Science Foundation to the San Diego group is acknowledged. Two of us (S.B. and F.R.) would like to thank the Digital Equipment Corporation for support. And finally, we are grateful to the staff of the SPS, and in particular to N. Doble, for the excellent beam conditions and assistance provided during our tests.

REFERENCES

1. G. Jarlskog and D. Rein (eds.), Proc. Large Hadron Collider Workshop, Aachen 1990, Vols. I, II, III, CERN 90-10/ECFA 90-133.
2. The L* Collaboration, Letter of Intent to the SSC (1991).
3. R. DeSalvo *et al.*, Nucl. Instr. and Meth. **A279** (1989) 467.
4. D. Acosta *et al.*, Nucl. Instr. and Meth. **A294** (1990) 193.
5. D. Acosta *et al.*, Nucl. Instr. and Meth. **A302** (1991) 36.
6. D. Acosta *et al.*, Nucl. Instr. and Meth. **A305** (1991) 55.
7. D. Acosta *et al.*, Nucl. Instr. and Meth. **B62** (1991) 116.
8. D. Acosta *et al.*, Nucl. Instr. and Meth. **A308** (1991) 481.
9. D. Acosta *et al.*, Nucl. Instr. and Meth. **A309** (1991) 143.
10. D. Acosta *et al.*, The performance of a lead/scintillating-fiber calorimeter at LHC/SSC compatible gate widths, CERN preprint CERN-PPE/91-195, to be published in Nucl. Instr. and Meth.
11. R. Wigmans, Nucl. Instr. and Meth. **A259** (1987) 389.
12. E. Bernardi *et al.*, Nucl. Instr. and Meth. **A262** (1987) 229.
13. T. Åkesson *et al.*, Nucl. Instr. and Meth. **A262** (1987) 243.
14. J.E. Moyal, Phil. Mag. **46** (1955) 263; E. Bernardi, Internal report DESY/ F1-87-01 (unpublished), DESY, Hamburg.
15. R. Wigmans, Performance and Limitations of Hadron Calorimeters, Proc. of the 2nd Int. Conf. on Calorimetry in High Energy Physics, Capri (I), 1991; preprint CERN-PPE/91-205 (1991).
16. Particle Data Group, Phys. Lett. **B239** (1990), page III 5,6.
17. W. Lohmann, R. Kopp and R. Voss, Energy loss of muons in the energy range 1 GeV to 10 TeV, CERN yellow report 85-03 (1985).
18. R. Brun *et al.*, GEANT-CERN Program Library, W 5013, version 3.14.
19. Particle Data Group, Phys. Lett. **B170** (1986) 38.

FIGURE CAPTIONS

1. Detail of the front face of the calorimeter (a) and the lateral structure of the C155 (b) and C20 (c) detectors, as seen by the particles entering the detector.
2. Layout of the beam line. See text for details
3. Characteristic energy deposit profile for a muon traversing the C20 leakage calorimeter. The signals in individual towers are given in units of pC (1/4 GeV).
4. Signal distributions for 5 GeV muons traversing the leakage calorimeter C20 perpendicularly. Shown are the signals distributions for the total leakage calorimeter (*a*) and for one of the towers (*b*). The calorimeter signals were converted into energy units using the calibration constants for electrons, not correcting for any instrumental effects (1 GeV = 4 pC).
5. The total C155 signal versus the fraction f_3 of the total signal recorded in the 3 *hottest* calorimeter towers, for 10 GeV particles.
6. Scatter plot of the signals in the C20 leakage calorimeter versus the signals in the C155 calorimeter, for 80 GeV particles. The pions and muons can be very clearly separated by a cut on the C155 signal. The calorimeter signals were converted into energy units using the calibration constants for electrons, not correcting for any instrumental effects (1 GeV = 4 pC).
7. Signal distributions for muons of 10, 20, 80 and 225 GeV traversing the 9.5 λ_I deep Spaghetti Calorimeter at $\theta_z = 3^0$. The calorimeter signals were converted into energy units using the calibration constants for electrons, not correcting for any instrumental effects (1 GeV = 4 pC).
8. The average and the most probable values for the energy loss as a function of the beam energy. The conversion of the signals (in pC) to energy (in GeV) was made on the basis of the calibration constants found with electrons, not correcting for any instrumental effect. Data for $\theta_z = 3^0$.
9. The fractional average energy loss $\overline{\Delta E_\mu}/E_\mu$ (*a*) and the spread in the fractional energy loss $\sigma_{\rm RMS}/E_\mu$ (*b*) as a function of the beam energy. The conversion of the signals (in pC) to energy (in GeV) was made on the basis of the calibration constants found with electrons, not correcting for any instrumental effect. Data for $\theta_z = 3^0$.
10. The average muon signals observed in the C20 calorimeter, as a function of the angle θ_z between the beam and the fiber axis. The calorimeter signals were converted into energy units using the calibration constants for electrons, not correcting for any instrumental effects (1 GeV = 4 pC). Data for 40, 80 and 225 GeV muons.

11. The ratio of the average muon signals at $\theta_z = 0^0$ and $\theta_z = 3^0$, as a function of the beam energy. Data for the C155 calorimeter (5, 10, 20, 40, 80 and 150 GeV) and for C20 (40, 80 and 225 GeV).

12. Detail of the calorimeter structure. Shown are the back plane and the fibers that stick out and are brought together in an hexagonal bunch in order to be read out. The cross section of the fiber bunch amounts to 23% of the lateral cross section of a tower. The bunch is centered on the tower axis.

13. Lateral cross section of the C155 area exposed in the matrix scan. Indicated are the tower boundaries, the exit points of the muon beams and the location of the fiber bunches. Points that were grouped together for the analysis are indicated with the same symbols (see also fig. 14).

14. The average muon signal as a function of the position of the exit point with respect to the horizontally nearest tower center. The 49 data sets corresponding to 49 different impact (exit) points were grouped together. The symbols for the experimental data points correspond to the ones in fig. 13.

15. Lateral cross section of the Spaghetti Calorimeter. Indicated are the approximate exit points of the muons in the angular scans and the location of the relevant fiber bunches.

16. The e/mip ratio as a function of the beam energy. See text for details.

17. Energy loss distributions for 20, 40 and 80 GeV muons in the 9.5 λ_I deep Spaghetti Calorimeter. The full circles represent the measured distributions, the histograms are the result of a GEANT Monte Carlo simulation. The energy scale is set by the calibration constants derived from the response to e.m. showers. The energy deposits found from the Monte Carlo were scaled up by a factor μ_S, listed in table 4. Data for $\theta_z = 3^0$.

TABLE CAPTIONS

1. Event statistics for the measurements with the C155 calorimeter. Listed are the beam energy, the angle between the muon beam and the fiber axis, the diameter of the beam spot on the calorimeter, the maximum energy deposit considered and the number of events.

2. The energy loss by muons traversing the 9.5 λ_I deep Spaghetti Calorimeter. For the different beam energies are listed the average and most probable energy loss values, the mean fraction of the muon energy absorbed by the calorimeter, the RMS width of the energy loss distribution and the fraction of the muon energy represented by this width. The calorimeter signals were converted into energy units using the calibration constants for electrons, not correcting for any instrumental effects (1 GeV = 4 pC). Data for $\theta_z = 0^0$ (a) and 3^0 (b). The 225 GeV results were obtained with the C20 calorimeter, for the other energies C155 was used.

3. Results of the determination of the e/mip ratio, based on an analysis of the average (table 3a) or most probable (table 3b) energy loss by muons traversing the calorimeter. The calculations are based on the fact that a minimum ionizing particle loses on average (most probably) 2.067 (1.882) GeV in the calorimeter, out of which 74.0 (63.3) MeV is deposited in the fibers. Shown for each beam energy are the energy loss measured on the basis of the e.m. shower calibration constants (table 2), the energy loss after correcting for the effects of light attenuation, the energy deposited in the fibers according to GEANT, the correction factor that has to be applied in order to calculate the measured energy deposit by a *mip* and the resulting e/mip value. See text for details. Data for $\theta_z = 3^0$.

4. The factor e/μ by which the nominal calibration constants, derived from the calorimeter response to e.m. showers, have to be multiplied in order to find the energy loss corresponding to a given muon signal. In order to find proper values for the average and the most probable energy losses and for the RMS width of the energy loss distribution, the corresponding numbers in table 2 have to be multiplied by this factor. The factor is the inverse of the factor μ_S, found by comparing the measured and simulated signal distributions (see text) and also listed, multiplied by the average ratio of an electron and muon signal that would be equivalent in the absence of light attenuation in the fibers (0.85, see text).

Table 1 Event statistics C155 measurements				
E_μ (GeV)	θ_z	Area	E_{cut} (GeV)	# Muons
5	0^0	ϕ 10 cm	-	143
5	3^0	ϕ 10 cm	-	140
10	0^0	ϕ 2 cm	-	271
10	3^0	ϕ 2 cm	-	233
20	0^0	ϕ 2 cm	-	668
20	3^0	ϕ 2 cm	-	888
40	0^0	ϕ 2 cm	< 30	71
40	3^0	ϕ 2 cm	< 30	452
80	0^0	ϕ 2 cm	< 60	79
80	3^0	ϕ 2 cm	< 60	69
150	0^0	ϕ 2 cm	< 100	45
150	3^0	ϕ 2 cm	< 100	44
80	2^0	24×24 cm^2	< 60	1500

Table 2a Energy loss by muons, $\theta_z = 0^0$					
E_μ (GeV)	$\overline{\Delta E_\mu}$ (GeV)	ΔE_μ (GeV) (mop)	$\overline{\Delta E_\mu}/E_\mu$ (%)	σ_{RMS} (GeV)	$\sigma_{\mathrm{RMS}}/E_\mu$ (%)
5	3.91 ± 0.09	3.31 ± 0.09	78.2 ± 1.8	1.06 ± 0.06	26.1 ± 1.2
10	4.26 ± 0.08	3.48 ± 0.08	42.6 ± 0.8	1.29 ± 0.06	12.9 ± 0.6
20	5.03 ± 0.09	3.38 ± 0.08	25.6 ± 0.5	2.28 ± 0.06	11.4 ± 0.3
40	6.31 ± 0.38	5.01 ± 0.23	15.7 ± 1.0	3.20 ± 0.27	8.0 ± 0.7
80	8.62 ± 0.96	7.01 ± 0.22	10.7 ± 1.2	8.55 ± 0.68	10.6 ± 0.9
150	10.70 ± 1.49	7.91 ± 0.26	7.1 ± 1.0	10.0 ± 1.1	6.7 ± 0.7
225	11.55 ± 0.29	6.82 ± 0.07	5.1 ± 0.2	15.6 ± 0.2	6.9 ± 0.1

Table 2b Energy loss by muons, $\theta_z = 3^0$					
E_μ (GeV)	$\overline{\Delta E_\mu}$ (GeV)	ΔE_μ (GeV) (mop)	$\overline{\Delta E_\mu}/E_\mu$ (%)	σ_{RMS} (GeV)	$\sigma_{\mathrm{RMS}}/E_\mu$ (%)
5	3.80 ± 0.07	3.35 ± 0.07	76.0 ± 1.4	0.85 ± 0.05	16.8 ± 1.0
10	4.07 ± 0.07	3.48 ± 0.07	40.6 ± 0.7	1.01 ± 0.05	10.1 ± 0.5
20	4.39 ± 0.05	3.61 ± 0.05	21.9 ± 0.3	1.53 ± 0.04	7.6 ± 0.2
40	4.96 ± 0.12	3.66 ± 0.08	12.0 ± 0.3	2.49 ± 0.08	6.2 ± 0.2
80	6.44 ± 0.34	4.10 ± 0.10	8.0 ± 0.4	6.51 ± 0.24	8.1 ± 0.3
150	7.97 ± 1.42	5.14 ± 0.46	5.3 ± 1.0	9.41 ± 1.0	6.2 ± 0.7
225	9.98 ± 0.28	5.48 ± 0.06	4.4 ± 0.2	15.9 ± 0.2	7.0 ± 0.1

Table 3a Determination of the e/mip ratio (from $< dE/dx >$)					
E_μ (GeV)	$\overline{\Delta E_\mu}$ (GeV)	$\overline{\Delta E_\mu}(\lambda_{att} = \infty)$	$\overline{\Delta E}_{fiber}$ (MeV,MC)	$\overline{\Delta E}_{fiber}/\overline{\Delta E}_{mip}$	e/mip
5	3.80 ± 0.07	3.23 ± 0.06	82.1 ± 0.5	1.109 ± 0.006	0.710 ± 0.013
10	4.07 ± 0.07	3.46 ± 0.05	88.6 ± 0.6	1.198 ± 0.007	0.715 ± 0.012
20	4.39 ± 0.05	3.73 ± 0.04	97.9 ± 1.0	1.323 ± 0.014	0.733 ± 0.010
40	4.96 ± 0.12	4.22 ± 0.10	107.4 ± 1.4	1.451 ± 0.019	0.712 ± 0.010
80	6.44 ± 0.34	5.47 ± 0.29	131.2 ± 2.5	1.773 ± 0.031	0.669 ± 0.030
150	7.97 ± 1.42	6.77 ± 1.21	171.0 ± 5.7	2.315 ± 0.075	0.705 ± 0.124
225	9.98 ± 0.28	8.48 ± 0.24	221.9 ± 7.4	3.003 ± 0.099	0.731 ± 0.034

Table 3b Determination of the e/mip ratio (from dE/dx^{mop})					
E_μ (GeV)	$\Delta E_\mu^{\mathrm{mop}}$ (GeV)	$\Delta E_\mu^{\mathrm{mop}}(\lambda_{att} = \infty)$	$\Delta E_{fiber}^{\mathrm{mop}}$ (MeV,MC)	$\Delta E_{fiber}^{\mathrm{mop}}/\Delta E_{mip}^{\mathrm{mop}}$	e/mip
5	3.35 ± 0.07	2.85 ± 0.06	66.0 ± 0.5	1.043 ± 0.008	0.689 ± 0.015
10	3.48 ± 0.07	2.96 ± 0.06	70.2 ± 0.4	1.109 ± 0.006	0.705 ± 0.015
20	3.61 ± 0.05	3.07 ± 0.04	71.6 ± 0.7	1.131 ± 0.012	0.694 ± 0.012
40	3.66 ± 0.08	3.11 ± 0.07	74.0 ± 0.9	1.170 ± 0.014	0.707 ± 0.018
80	4.10 ± 0.10	3.49 ± 0.09	85.4 ± 0.9	1.350 ± 0.014	0.728 ± 0.019
150	5.14 ± 0.46	4.37 ± 0.39	102.2 ± 2.0	1.616 ± 0.031	0.695 ± 0.064
225	5.48 ± 0.06	4.66 ± 0.05	120.2 ± 1.6	1.898 ± 0.025	0.767 ± 0.013

Table 4 Calibration constants for muons		
E_μ (GeV)	μ_S	e/μ
5	1.25 ± 0.03	0.68 ± 0.02
10	1.20 ± 0.03	0.71 ± 0.02
20	1.23 ± 0.03	0.69 ± 0.02
40	1.23 ± 0.03	0.69 ± 0.02
80	1.15 ± 0.07	0.74 ± 0.05
150	0.98 ± 0.17	0.87 ± 0.15
225	0.96 ± 0.05	0.88 ± 0.05

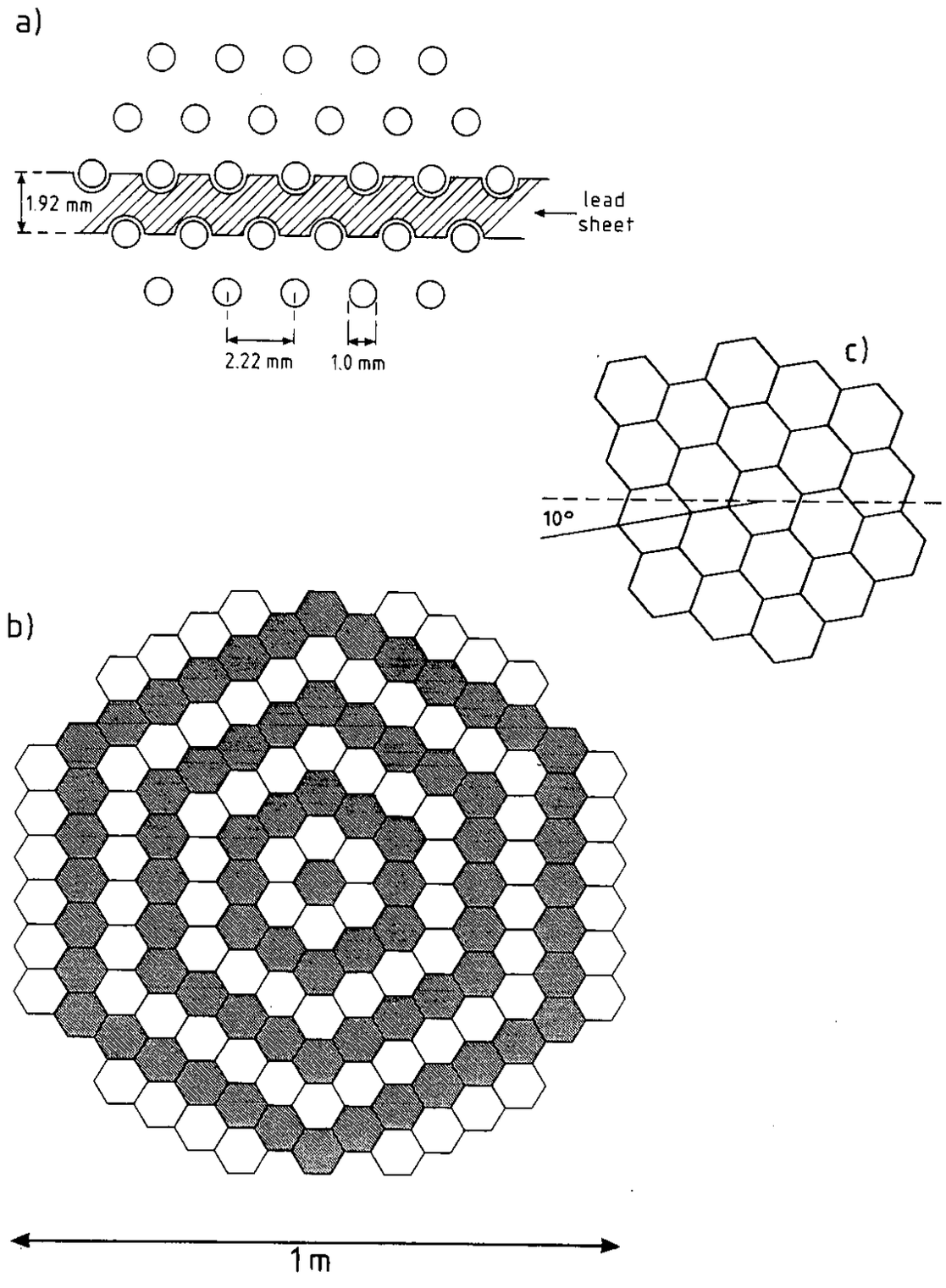

Figure 1

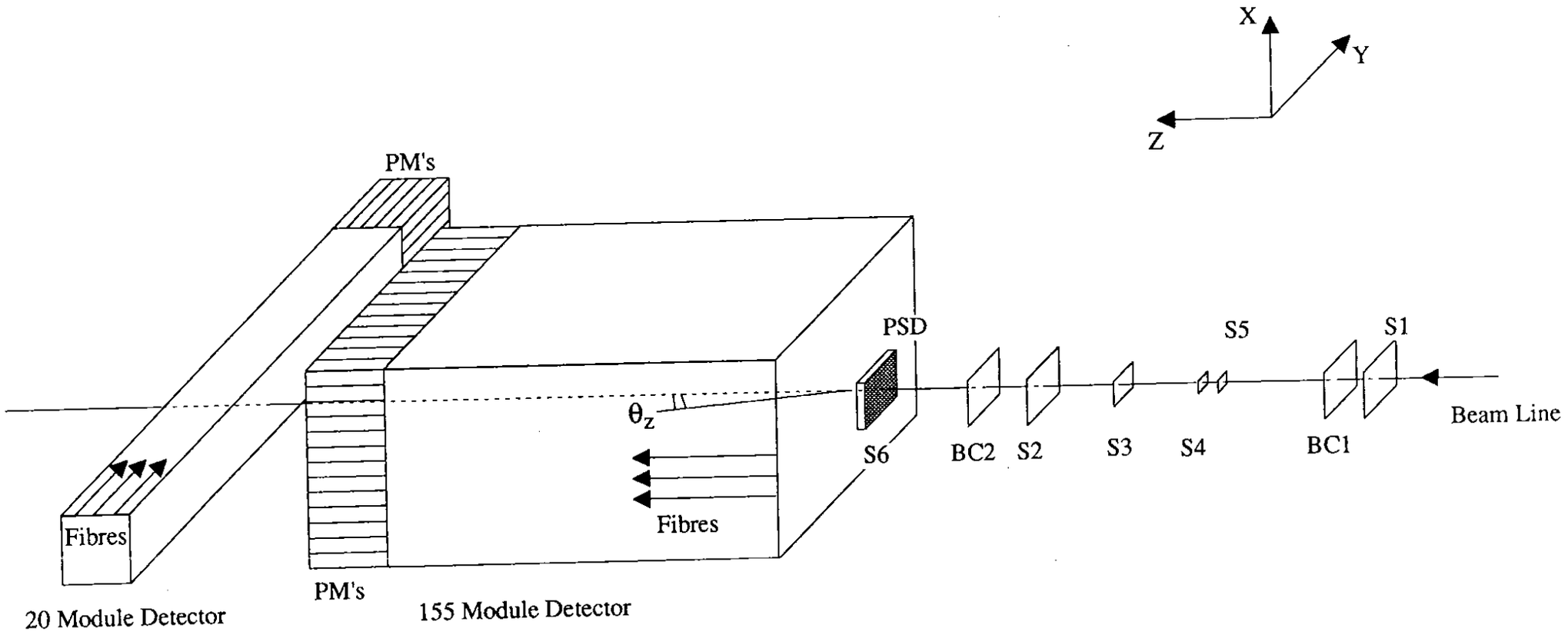

Not to scale

Figure 2

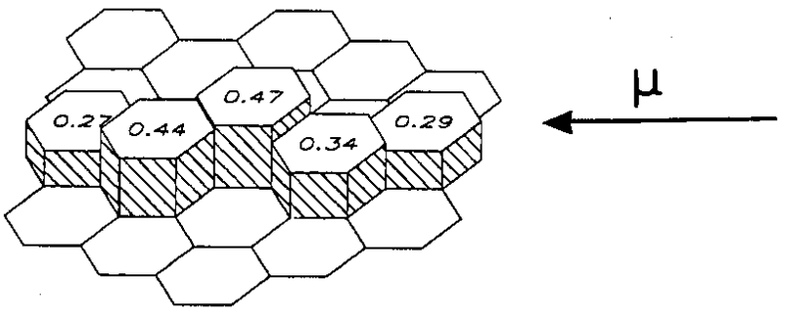

Figure 3

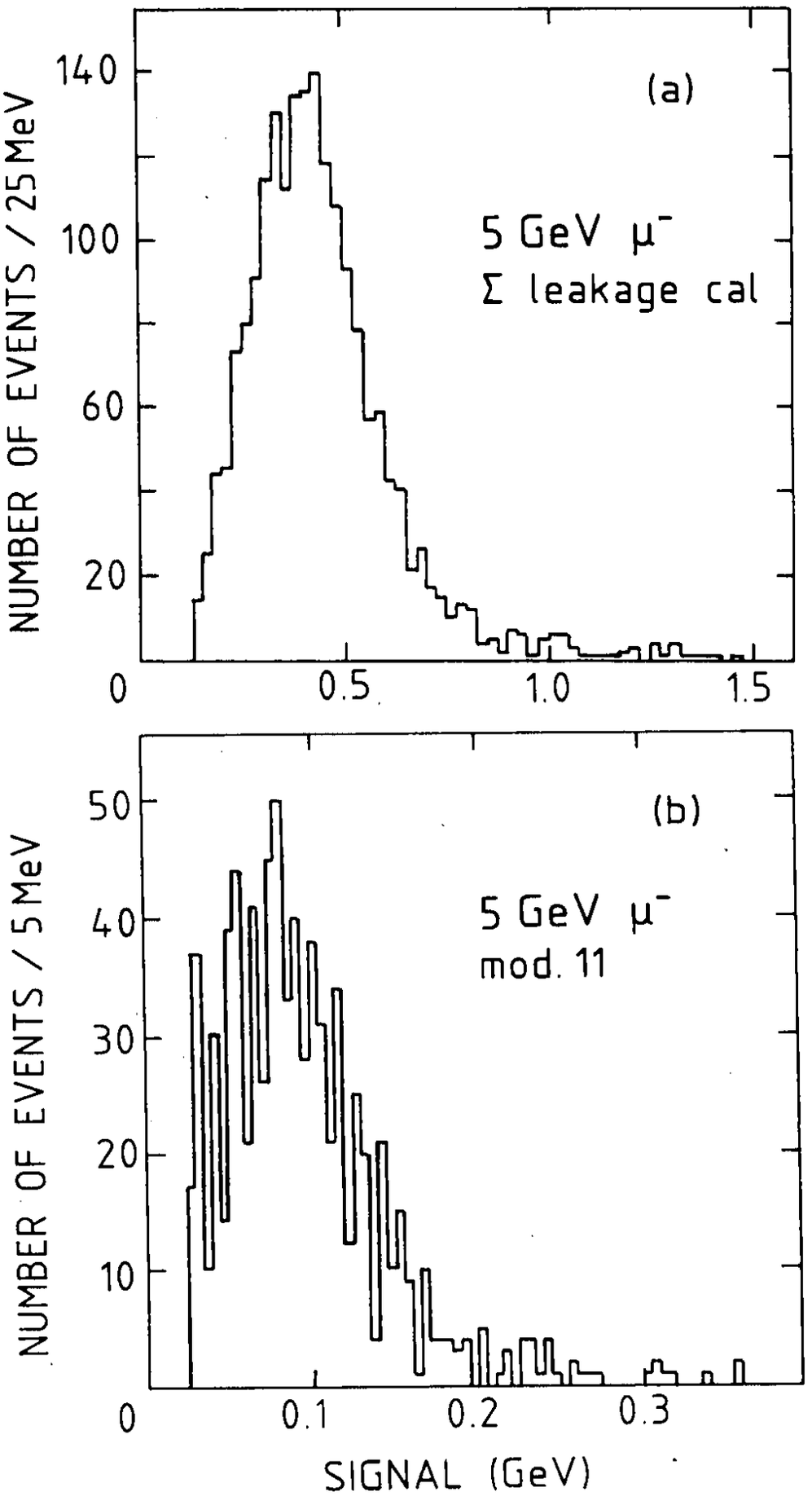
(a)
5 GeV μ⁻
Σ leakage cal
NUMBER OF EVENTS / 25 MeV
140
100
60
20
0
0.5
1.0
1.5
(b)
5 GeV μ⁻
mod. 11
NUMBER OF EVENTS / 5 MeV
50
40
30
20
10
0
0.1
0.2
0.3
SIGNAL (GeV)

Figure 4

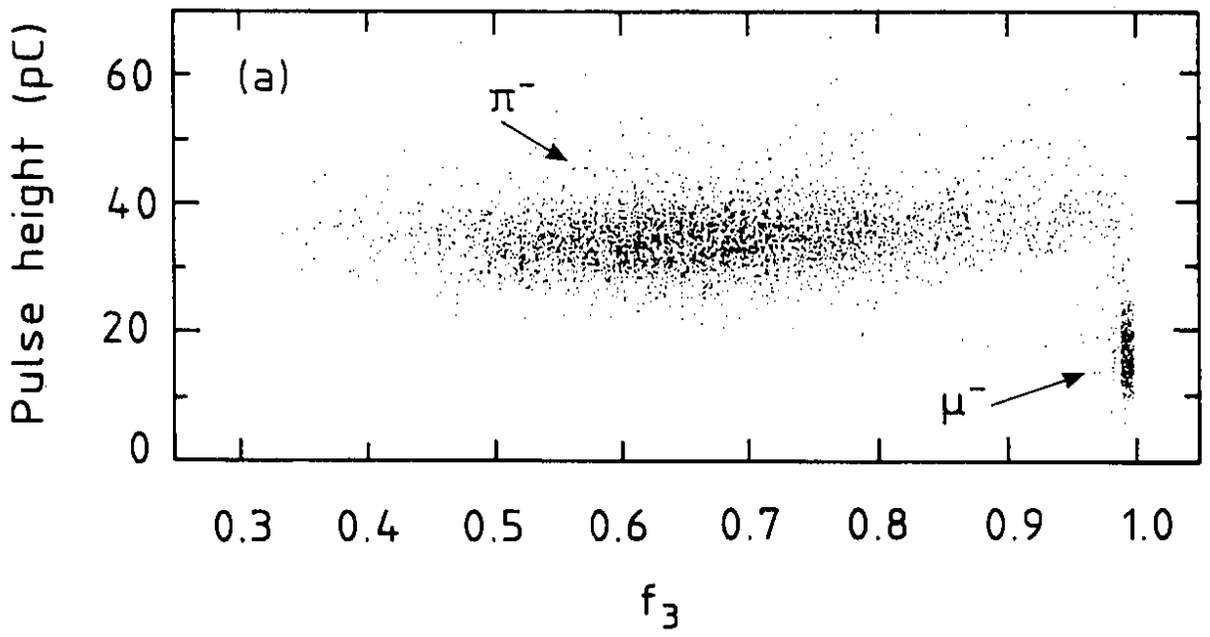

Figure 5

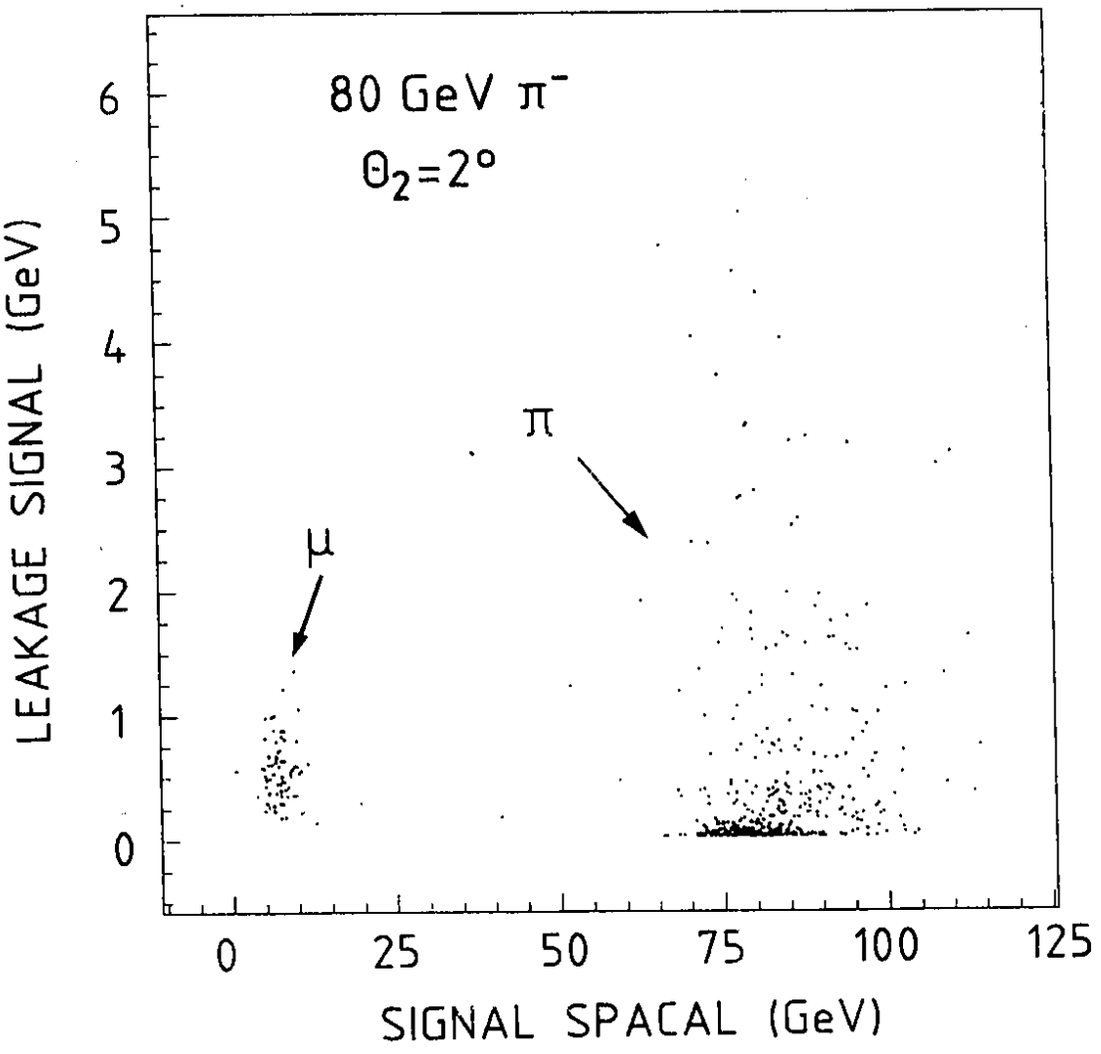
80 GeV π⁻
Θ2=2°
μ
π
LEAKAGE SIGNAL (GeV)
SIGNAL SPACAL (GeV)
0
1
2
3
4
5
6
0
25
50
75
100
125

Figure 6

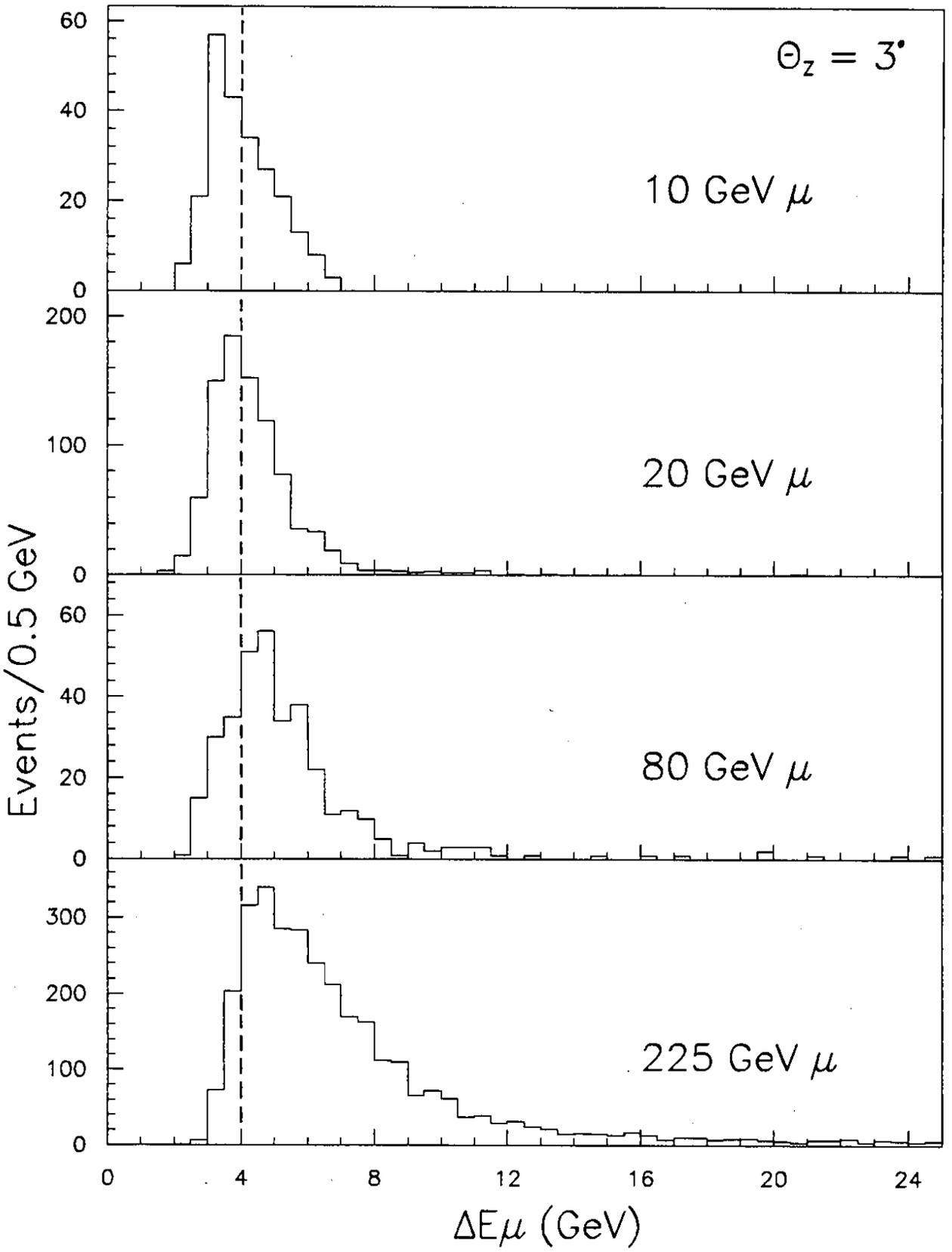
$\Theta_z = 3^\circ$
10 GeV μ
20 GeV μ
80 GeV μ
225 GeV μ
Events/0.5 GeV
$\Delta E\mu$ (GeV)
0
4
8
12
16
20
24
60
40
20
200
100
300

Figure 7

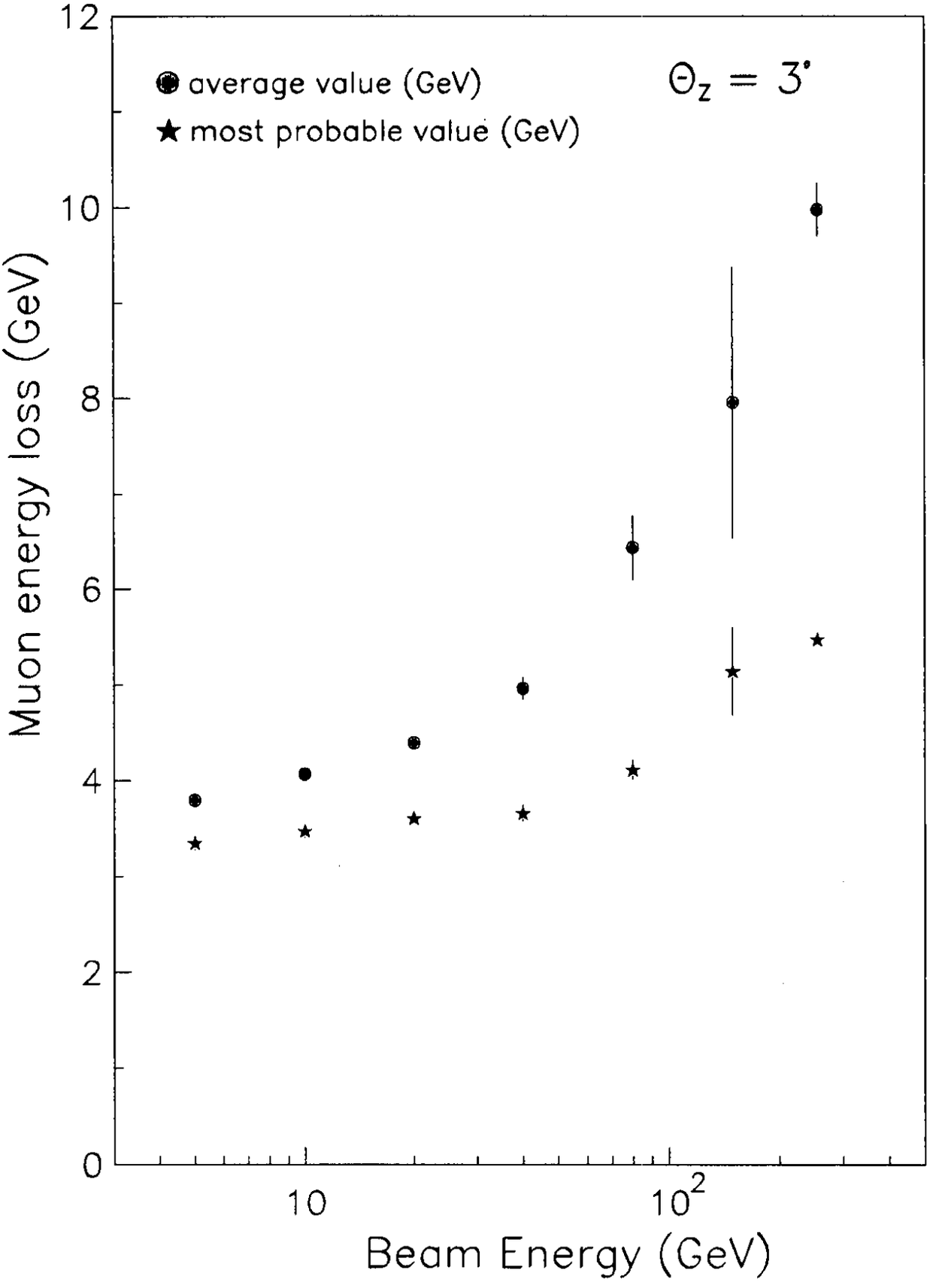
average value (GeV)
most probable value (GeV)
$\Theta_z = 3^\circ$
Muon energy loss (GeV)
Beam Energy (GeV)
0
2
4
6
8
10
12
10
10^2

Figure 8

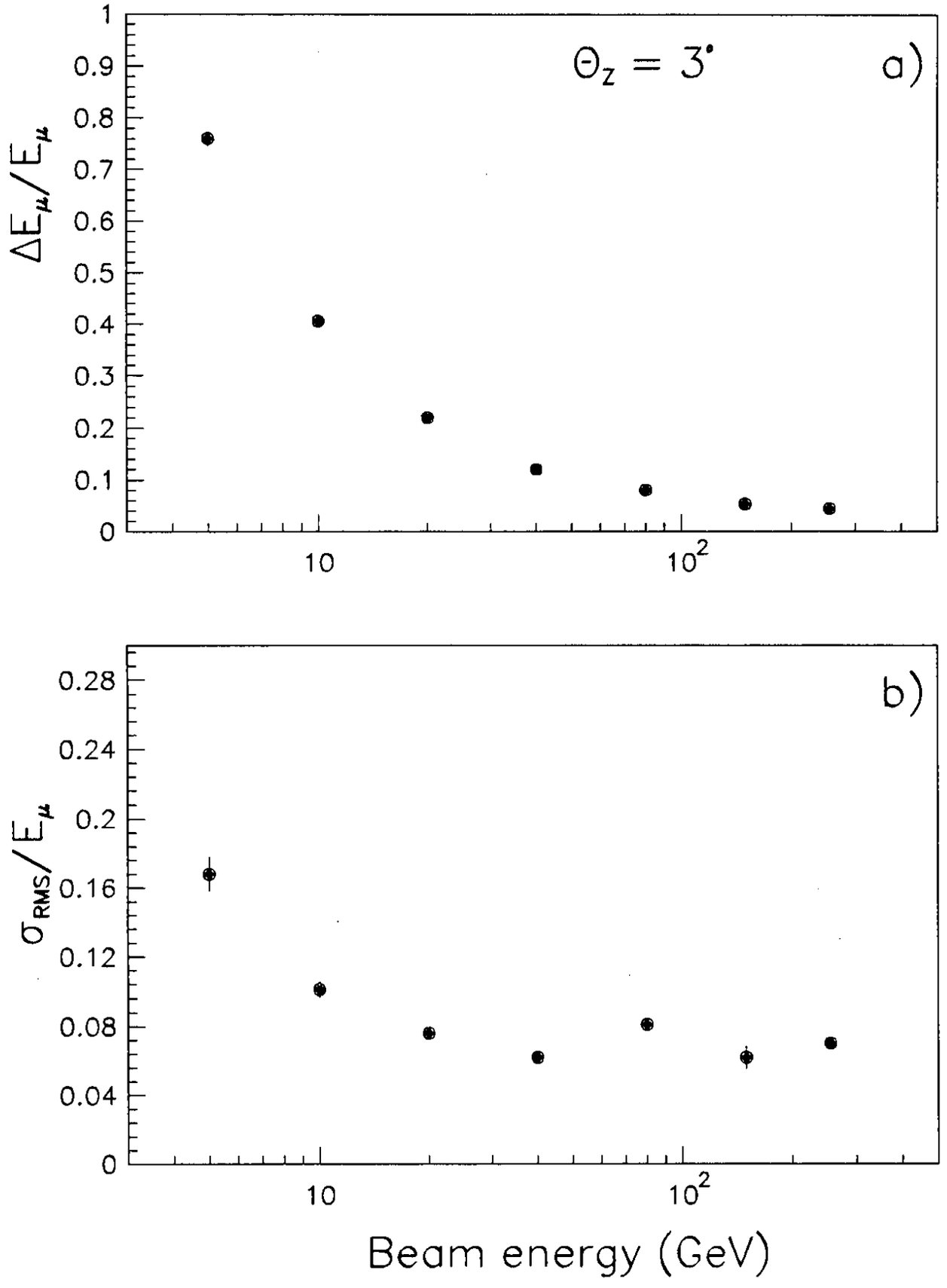
$\Theta_z = 3^\circ$
a)
$\Delta E_\mu / E_\mu$
1
0.9
0.8
0.7
0.6
0.5
0.4
0.3
0.2
0.1
0
10
10^2
b)
σ_{RMS} / E_μ
0.28
0.24
0.2
0.16
0.12
0.08
0.04
0
10
10^2
Beam energy (GeV)

Figure 9

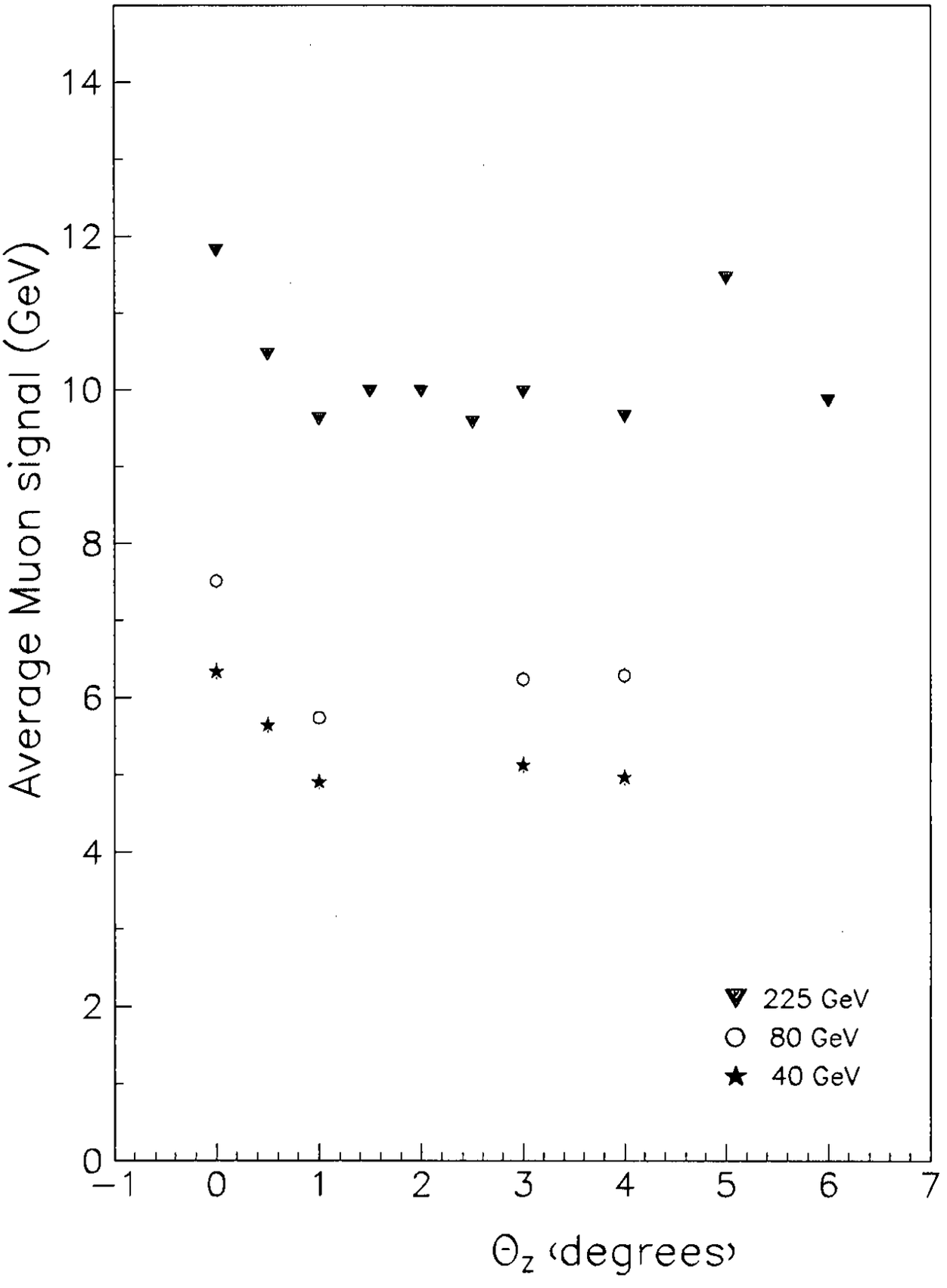
Average Muon signal (GeV)
14
12
10
8
6
4
2
0
−1
0
1
2
3
4
5
6
7
Θ_z ‹degrees›
225 GeV
80 GeV
40 GeV

Figure 10

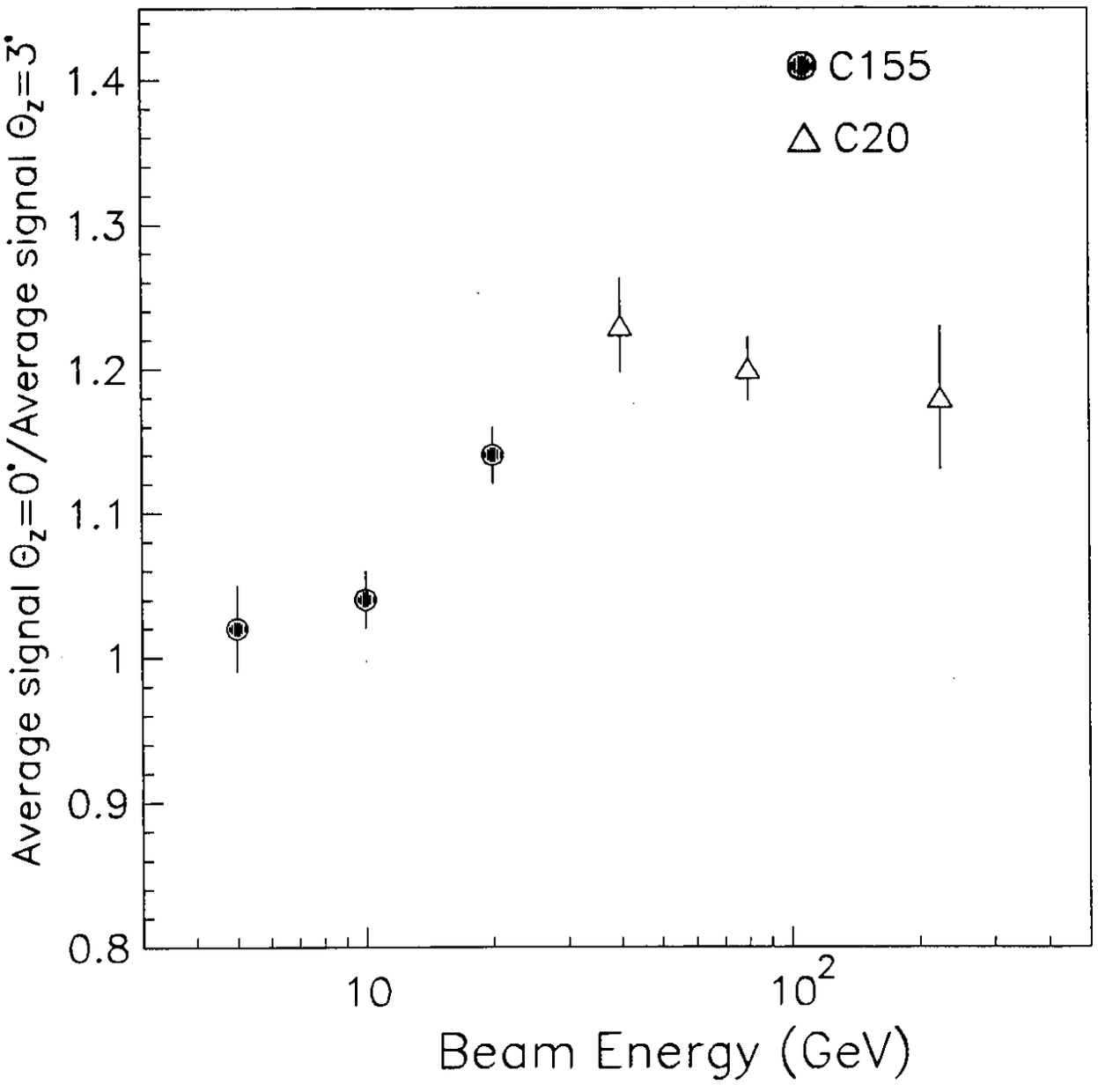
C155
C20
Average signal $\Theta_z=0^\circ$/Average signal $\Theta_z=3^\circ$
1.4
1.3
1.2
1.1
1
0.9
0.8
10
10^2
Beam Energy (GeV)

Figure 11

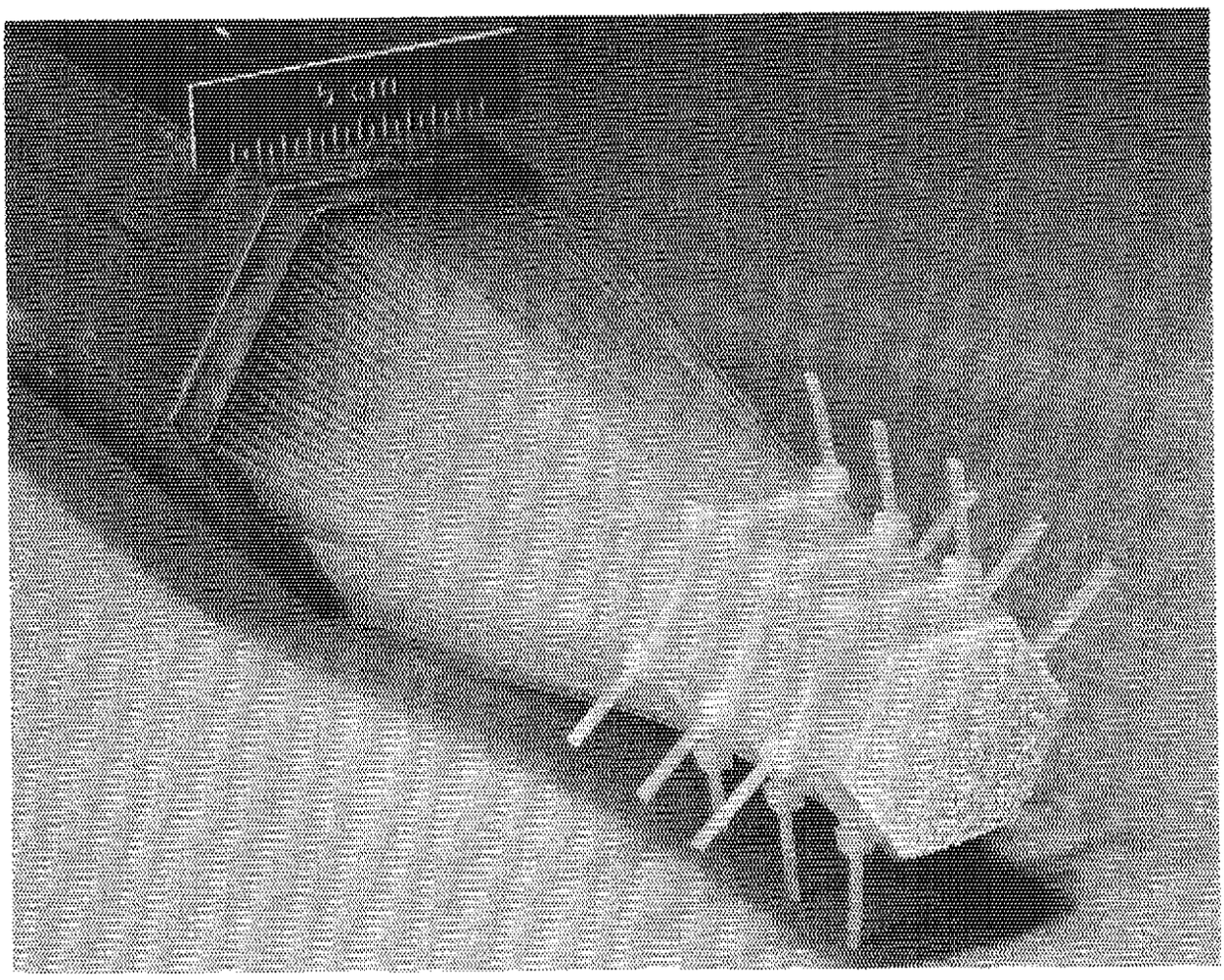

Figure 12

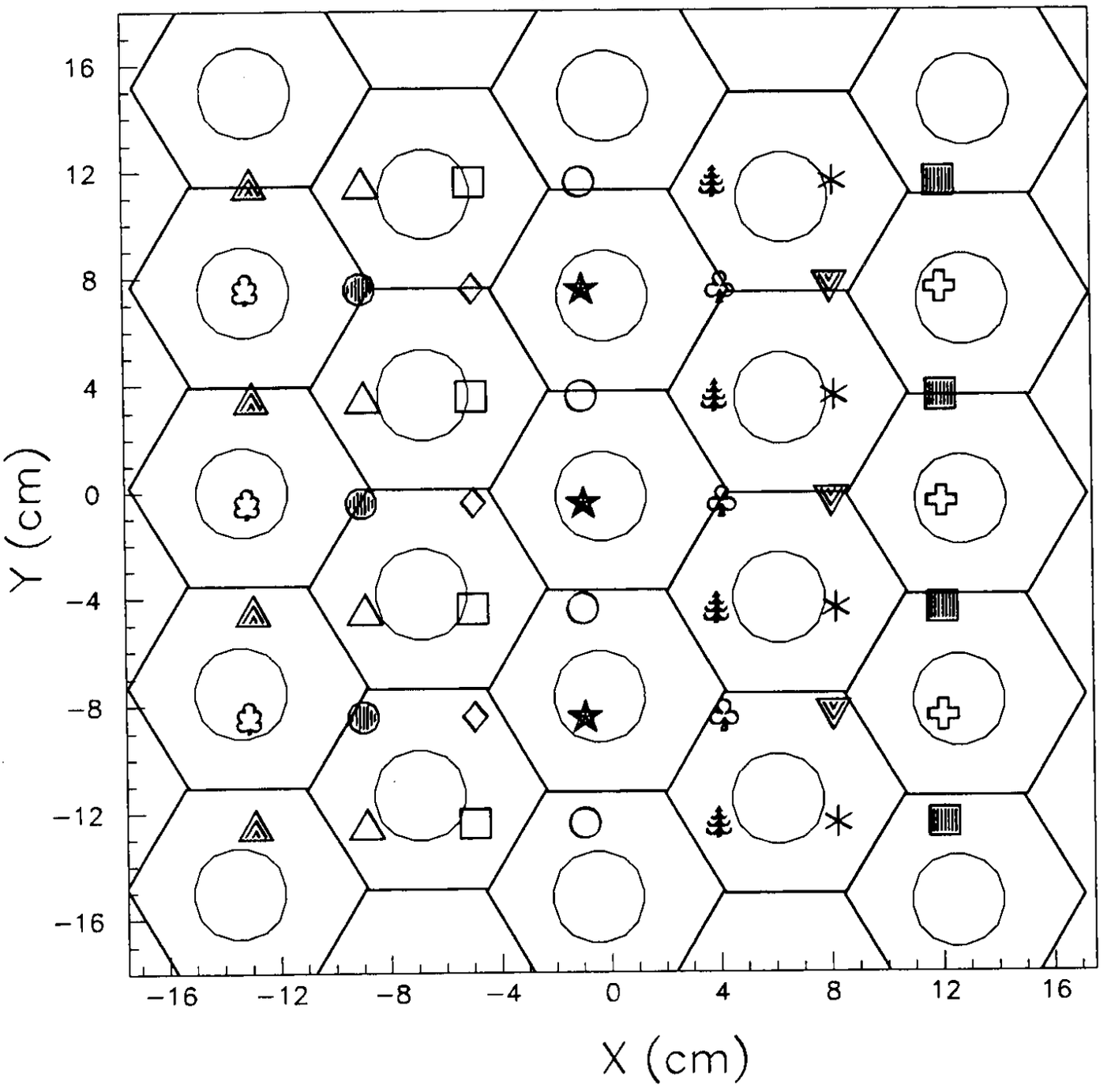

Figure 13

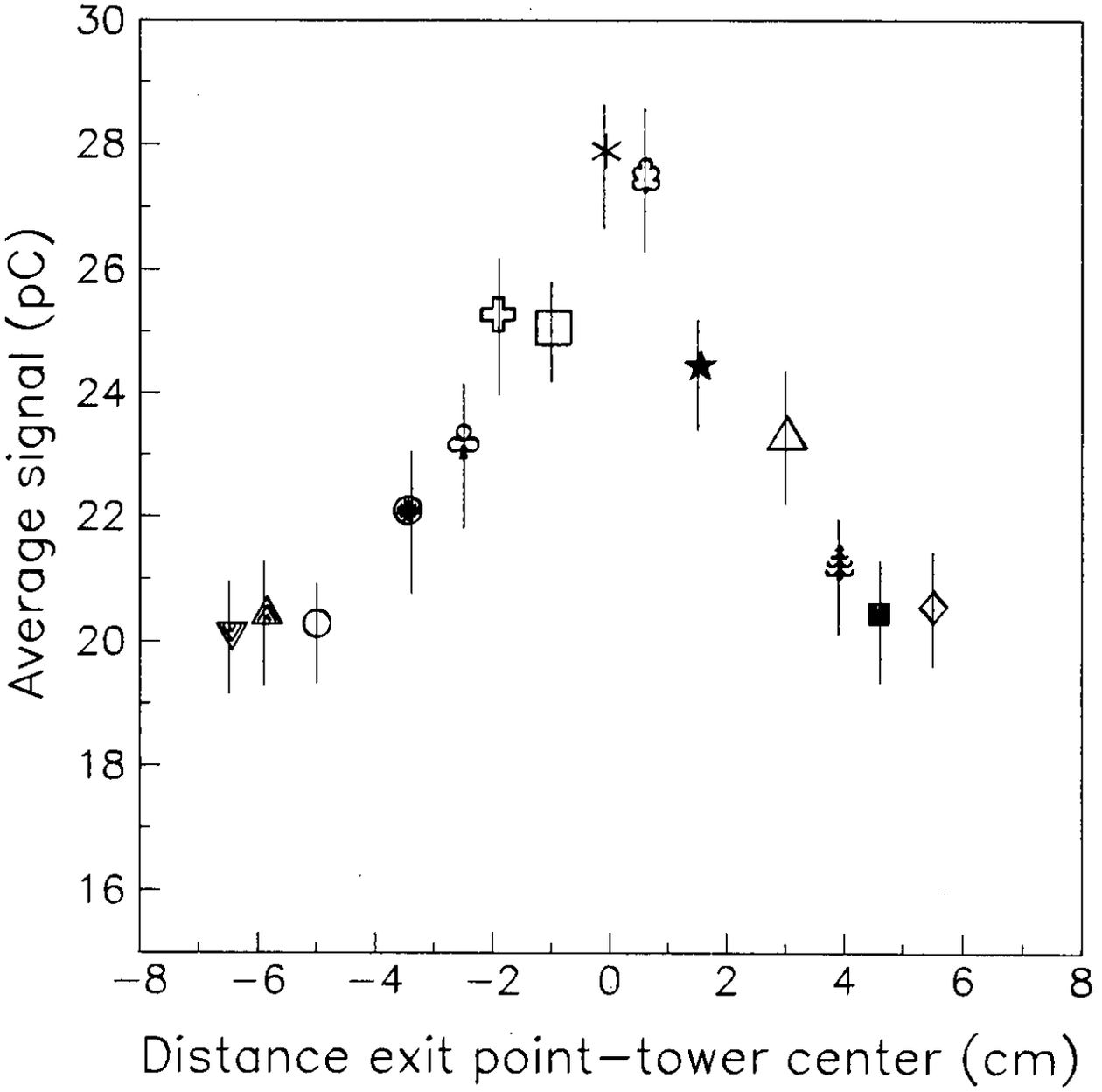
30
28
26
24
22
20
18
16
Average signal (pC)
−8
−6
−4
−2
0
2
4
6
8
Distance exit point−tower center (cm)

Figure 14

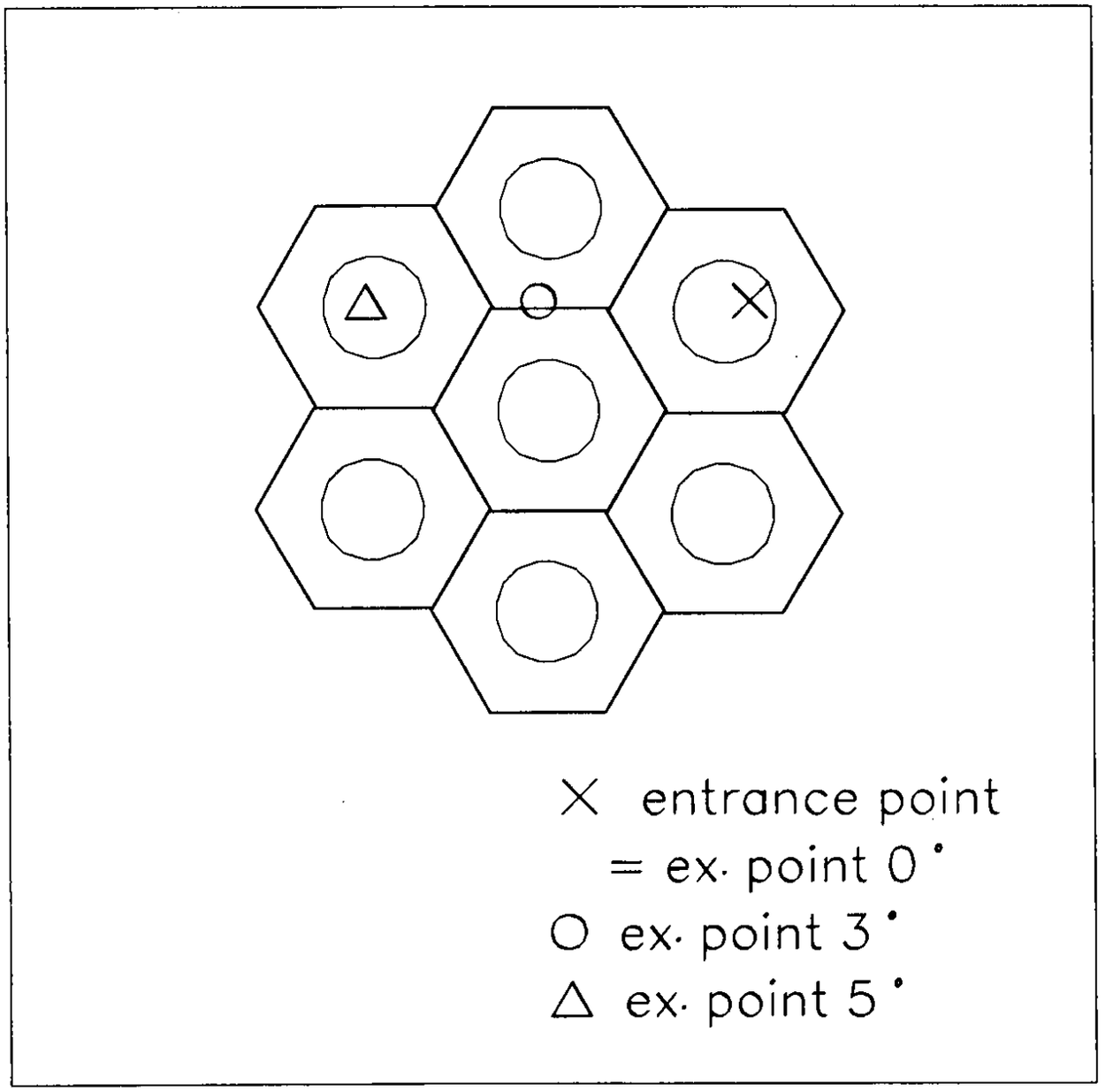

Figure 15

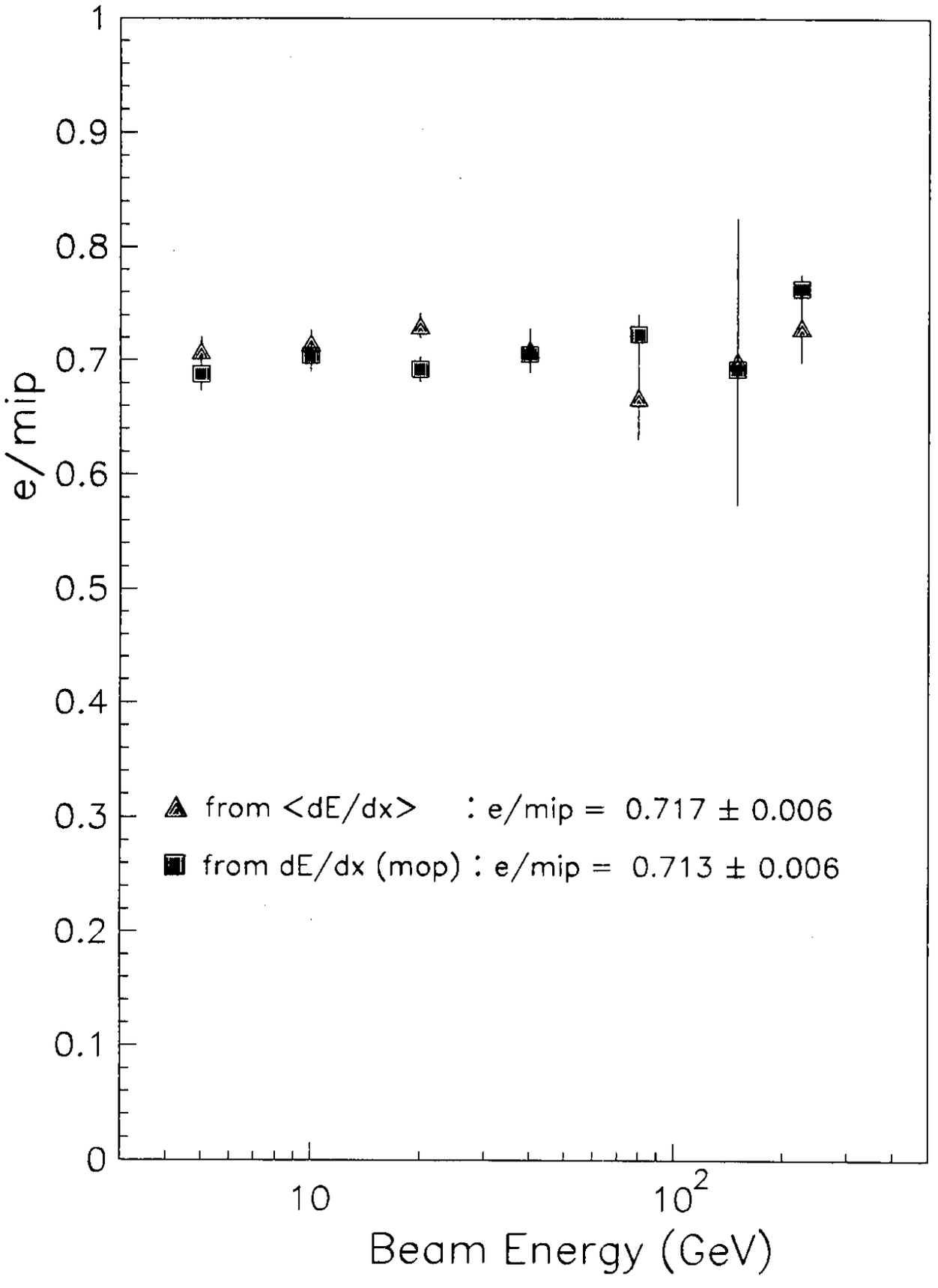
1
0.9
0.8
0.7
0.6
0.5
0.4
0.3
0.2
0.1
0
e/mip
from <dE/dx> : e/mip = 0.717 ± 0.006
from dE/dx (mop) : e/mip = 0.713 ± 0.006
10
10^2
Beam Energy (GeV)

Figure 16

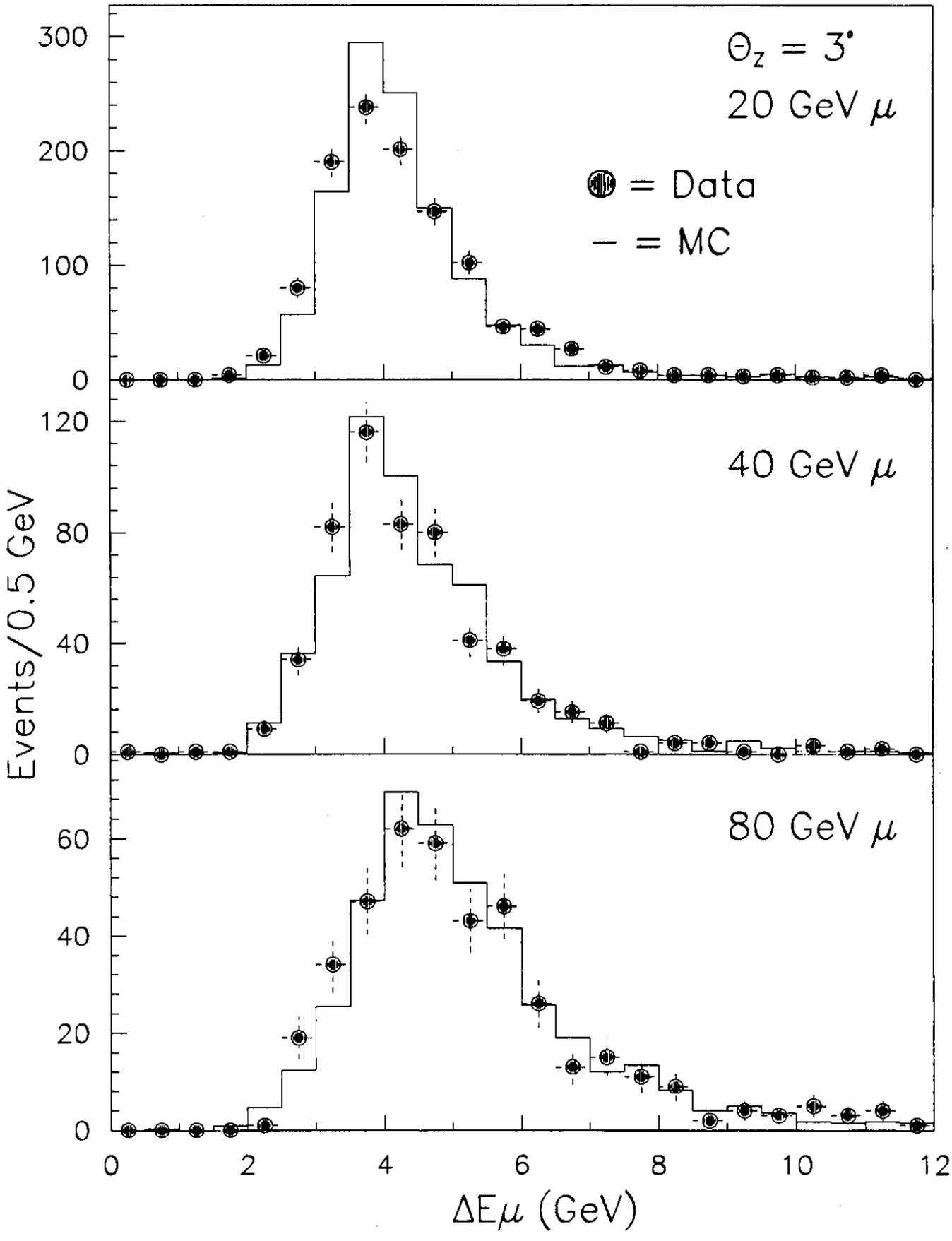
$\Theta_z = 3^\circ$
20 GeV μ
= Data
= MC
40 GeV μ
80 GeV μ
Events/0.5 GeV
$\Delta E\mu$ (GeV)
300
200
100
0
120
80
40
0
60
40
20
0
0
2
4
6
8
10
12

Figure 17